Available online at www.sciencedirect.com
SCIENCE DIRECT®
ELSEVIER
Palaeogeography, Palaeoclimatology, Palaeoecology 230 (2006) 85–128
PALAEO
www.elsevier.com/locate/palaeo

Record of palaeoenvironmental changes in a Lower Permian organic-rich lacustrine succession: Integrated sedimentological and geochemical study of the Rudník member, Krkonoše Piedmont Basin, Czech Republic

Karel Martínek [a,*], Martin Blecha [b], Vilém Daněk [a], Jiří Franců [c], Jana Hladíková [d], Renata Johnová [e], David Uličný [f]

[a] *Institute of geology and palaeontology, Charles University, Albertov 6, 128 43 Prague 2, Czech Republic*
[b] *HYDROTECH SG, s.r.o., Přemyslova 6, 128 00 Praha 2, Czech Republic*
[c] *Energy and Geoscience Institute, University of Utah, Salt Lake City, USA*
[d] *Czech Geological Survey, Klárov 3, P.O.Box 85, 118 21 Prague 1, Czech Republic*
[e] *Department of Geochemistry, Mineralogy and Mineral Resources, Charles University, Albertov 6, 128 43 Prague 2, Czech Republic*
[f] *Department. of Earth Sciences, The University of Western Ontario, London, Ontario, N6A 5B7, Canada*

Received 24 June 2004; received in revised form 13 July 2005; accepted 18 July 2005

Abstract

This study presents an integrated sedimentological and geochemical analysis of the Lower Permian Rudník member — the most extensive lacustrine deposits in the Krkonoše Piedmont Basin. Grey to black and variegated lacustrine mudstones, laminites and carbonates of the Rudník member have a lateral extent of more than 400 km^2. In the studied sections four facies associations were recognised: A) anoxic offshore, B) suboxic to oxic offshore, C) nearshore and mudflat, and D) slope deposits. In the northern part of the E–W elongated basin, anoxic to suboxic organic-rich offshore lacustrine facies dominate and form a succession up to 130 m thick. Fan-delta and turbidite facies occur locally along the faulted northern basin margin. The central part of the basin is occupied by anoxic to oxic offshore facies interfingering with nearshore carbonate and mudflat facies of the low-gradient lacustrine margin. In the central part of the basin, the thickness of the lacustrine deposits of the Rudník member reaches up to 60–70 m. In the southern part of the basin fluvial and alluvial plain facies dominate and alternate with minor lacustrine nearshore facies. The lateral facies distribution indicates that subsidence along the northern basin fault was the main mechanism generating the asymmetric infill geometry in the basin's half-graben setting.

The δ^{18}O values of primary and early diagenetic calcite range between −11.0‰ and +1.3‰ (V-PDB) and δ^{13}C values between −5.1‰ and +3.7‰; most of the data fall within the range of freshwater limestones. Coarser-grained pure microspar laminae show more positive δ^{13}C values in comparison to clayey organic-rich micrite laminae, and are interpreted as a record of bioinduced precipitation during seasonal eutrophication. The obtained $\delta^{13}C_{TOC}$ values range from −29.0‰ to −24.0‰, the

* Corresponding author. Tel.: +420 2195 1464; fax: +420 2195 1452.
E-mail address: karel@natur.cuni.cz (K. Martínek).

0031-0182/$ - see front matter
doi:10.1016/j.palaeo.2005.07.009

total organic carbon (TOC) content from 0.26% to 23%. Maceral analysis and Rock-Eval pyrolysis indicate that most of the samples contain a mixture of aquatic and terrestrial organic matter, but two minor, distinctive groups of samples with algally-dominated and terrestrially-dominated organic matter composition, respectively, were also found. The study of vertical changes in boron content in the clay fraction of the lacustrine mudstones shows that high lake level stages were periods of lower salinity with the lowest boron contents (from 73 to 268 ppm), and periods of falling lake level were followed by significant increases in salinity with much higher boron values (293–603 ppm).

Lake-level fluctuations of the Rudník lacustrine system, which are recorded by shallowing-up units of sedimentary facies within most of the sections throughout the basin, can also be traced within the monotonous black shale dominated sections, where no sedimentological evidence of these lake level changes exists. Good indicators for such changes seem to be the $\delta^{18}O$ and $\delta^{13}C$ values of primary calcite, $\delta^{13}C_{TOC}$ and HI. These lake level fluctuations are interpreted as driven by climatic oscillations in the order of tens of thousands years, which could reflect climatic changes connected with the last glaciation event of Gondwana.

Keywords: Lower Permian; Bohemian Massif; Half-graben; Lacustrine facies; Lake level changes; Stable isotopes; Maceral analysis; Hydrogen index; Boron; Climate change

1. Introduction

Understanding the mechanisms driving stratigraphic architecture in continental deposits remains a matter of controversy and active research (e.g., Shanley and McCabe, 1994; Blair and Bilodeau, 1988; Sweet, 1999; Csato et al., 1997; Liro, 1993). The tectonic setting of the basin is one of the main factors determining basin-scale distribution of sedimentary facies within the basin (e.g., Alexander and Leeder, 1987; Soreghan and Cohen, 1996; Sánchez-Moya et al., 1996; Soreghan et al., 1999; Wells et al., 1999; Gawthorpe and Leeder, 2000). The interplay between tectonics, base level changes and climatically driven sediment supply can be very complex.

Lacustrine deposits are considered good palaeoenvironmental archives, which can record even high-frequency climatic changes. In the Dead Sea Basin, alluvial–lacustrine architecture can directly respond to lake-level changes (Csato et al., 1997). Sediment supply and lake-level variations have been closely coupled in Lakes Malawi and Tanganyika during the Quaternary (Scholz and Rosendahl, 1990). Significant climatic changes in the order of icehouse/greenhouse transitions are shown by the sedimentary and palaeontological record in the Upper Carboniferous and Lower Permian in different parts of Pangea (Gastaldo et al., 1996). Changes in the depositional environment can also be driven by tectonics. In the half-graben lake Tanganyika four structural basin margin types with characteristic facies associations were recognised (Soreghan and Cohen, 1996). Sánchez-Moya et al. (1996) linked the facies architecture of red beds in a Triassic half-graben to episodically changing rates of basin subsidence.

In thick lacustrine successions of cyclically stacked transgressive/regressive lithofacies, Milankovitch periodicities can be a good indicator of orbitally forced climate changes (Olsen and Kent, 1996; Fredriksen et al., 1998). However, in relatively thin successions dominated by monotonous offshore facies, the geochemistry of stable isotopes and organic matter must be taken in consideration in order to detect changes in lake-level and lake metabolism and to decipher their causes (Talbot, 1990; Talbot and Livingstone, 1989; Janaway and Parnell, 1989; Johnson et al., 1991; Gasse et al., 1989; Talbot and Johannessen, 1992; Ricketts and Johnson, 1996; Neumann et al., 2002; Stager et al., 2002; Johnson et al., 2000; Trauth et al., 2001; Bush et al., 2002). Such geochemical parameters can be good indicators of lake-level, hydrology and bioproductivity changes. Nevertheless in relatively thin successions, where time series analysis of the sedimentary and geochemical record cannot be done, the mechanisms causing lake-level and lake metabolism changes remain poorly understood. For example, during the last glacial maximum (~18 kyr BP) tropical African lakes contain evidence of major dry periods and low lake-levels, which are ascribed to weakening Afro-Asian monsoons (Stager et al., 2002). A similar pattern was found by Benson et al. (1998) in the mid-latitude

Mono Lake (California). Lake Tanganyika water-level fluctuation is in phase with glacio-eustatic sea-level changes and Gasse et al. (1989) hypothesised that water bound in ice caps resulted in low atmospheric moisture as a mechanism for the dry glacial periods. This explanation remains problematic, because equatorial lakes of northern Amazonia also show orbital forcing of lake-level but in the opposite phase relative to glacio-eustasy. The last glacial maximum 18–22 kyr BP was a wet time here and low lake-levels correlate with maximum insolation (Bush et al., 2002). This contradiction can be resolved by considering local changes in ocean and atmospheric circulation as the main mechanisms driving changes in local climate.

This paper discusses the sedimentary and geochemical record of a large lacustrine system of the earliest Permian age. The aim is to reconstruct the palaeogeography of the basin based on the lateral distribution of facies associations and to show the response of the large lake basin to different climatic and tectonic changes. To understand the interplay between changes in the hydrological regime, bioproductivity and palaeosalinity, which can show whether climate or tectonics were the main controlling factors, an integrated geochemical study of lacustrine carbonates, mudstones and organic matter was also carried out.

2. Geological background and lithostratigraphy

The Krkonoše Piedmont Basin (KPB) belongs to a system of post-orogenic extensional/transtensional basins which formed in the Bohemian Massif in the early post-orogenic phase, during the Westphalian and Saxonian times (about Moscovian to Sakmarian, c. 310–280 Ma) (Fig. 1). The basin was filled with non-marine red-beds of a total thickness of about 1800 m during the Upper Carboniferous and Lower Permian (Westphalian D–Sakmarian) Late Variscan extension/transtension (Fig. 2). There are several relatively thin grey to black shale, coaly, or variegated mudstone and carbonate interbeds penetrating the red bed infill, which are usually several tens of metres thick.

In the northern part of the basin the Lower Vrchlabí Formation of the Asselian age reaches a thickness of 350 m and is formed mainly by red brown alluvial/lacustrine mudstones with a lacustrine black shale interbed of the Rudník member (Fig. 2). In contrast, the basin's southern part is occupied by a much thinner succession (about 200 m) of red-brown alluvial/fluvial coarse-grained arkosic sandstones with minor interbeds of mudstones and conglomerates of the Stará Paka Sandstones (Prouza and Tásler, 2001). In the central part of the basin, the presence of inter-

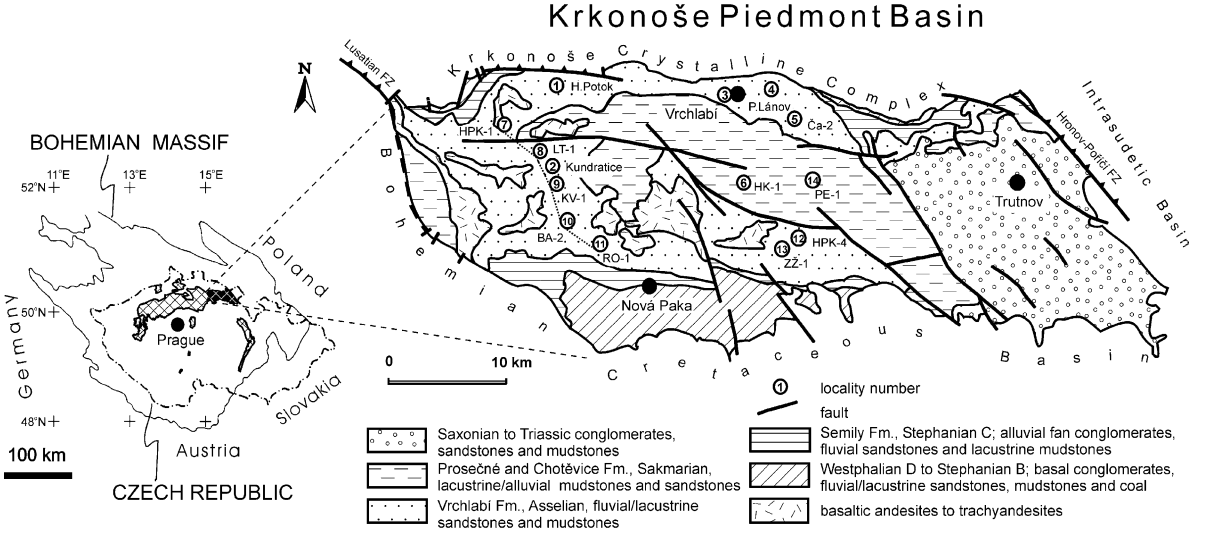

Fig. 1. Sketch map (left) showing the position of the Krkonoše Piedmont Basin on the NE part of the Bohemian Massif and other non-marine Upper Carboniferous and Permian basins. Simplified geological map (right) shows the location of the studied sections: 1) Honkův Potok, 2) Kundratice, 3) Vrchlabí, 4) Prostřední Lánov, 5) Čistá (Ča-2) and boreholes 6) HK-1, 7) HPK-1, 7) Kv-1, 8) Lt-1, 9) Kv-1, 10) Ba-2, 11) Ro-1, 12) HPK-4, 13) ZŽ-1, 14) Pe-1; line 7-8-9-10-11 is cross-section of Fig.3; FZ — fault zone.

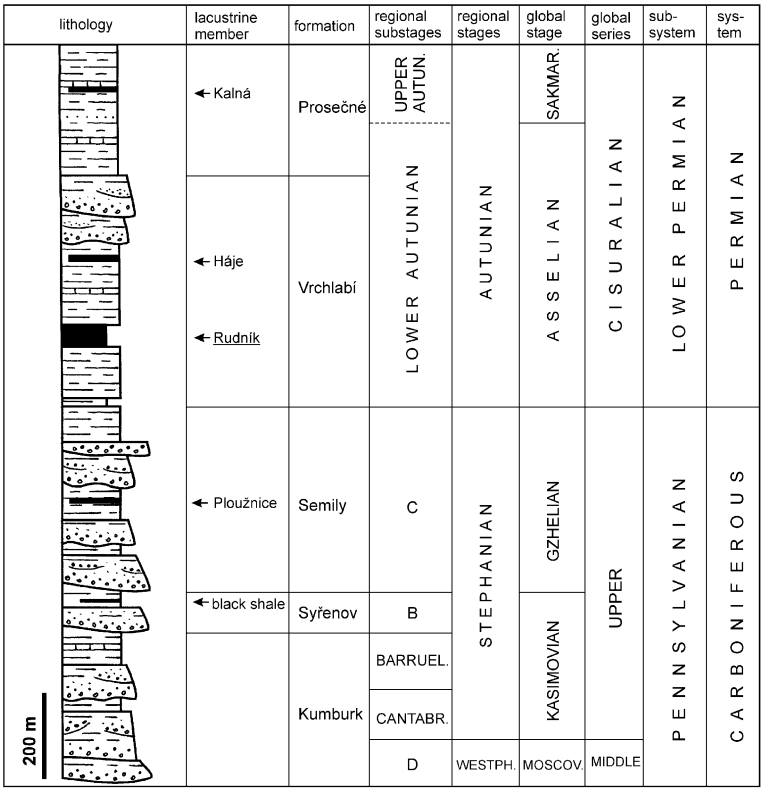

Fig. 2. Lithology and stratigraphy of the central part of the Krkonoše Piedmont Basin based on the borehole HK-1.

fingering variegated claystones, siltstones, carbonates and sandstones is typical and show common facies interfingering (Fig. 3).

The Rudník "Horizon" (= member in this paper) is defined by Tásler et al. (1981) and Prouza and Tásler (2001) as a 40–60 m thick succession of lacustrine grey mudstone with minor interbeds of black claystone, carbonate, sandstone and conglomerate, exposed mainly in the northern part of the basin. We use the term Rudník Lake deposits to describe deposits of the larger lacustrine system, which comprise suboxic and anoxic black, grey to variegated deposits of the Rudník member, and also the surrounding oxic red-brown lacustrine nearshore and alluvial facies closely related to lacustrine sedimentation. The Rudník Lake deposits cover an area of approximately 300–500 km^2 and along the northern basin margin deposits can reach a thickness of up to 130 m of grey to black shales. The areal extent is derived from the location of present-day outcrops, but could have been much larger, in the order of 1000 km^2. This estimate is based on post-sedimentary basin shortening, the assumption of occurrence in the eastern part of the basin, where the Vrchlabí Formation is covered by younger strata, and the finds of Rudník member equivalents in the adjacent Mnichovo Hradiště Basin, west of KPB (Prouza et al., 1997).

3. Sedimentary record

3.1. Approach and methods

Sedimentary facies of the Rudník Lake deposits were studied in detail in eight outcrop sections and five well cores; in this paper, four selected outcrop sections and one well core, representative of the main facies associations, are shown (Figs. 4–7; for locations see Fig. 1). Understanding the local sedimentological picture in a broader, basinwide stratigraphic framework was made possible by correlating gamma-ray and resistivity well logs, combined with the archive

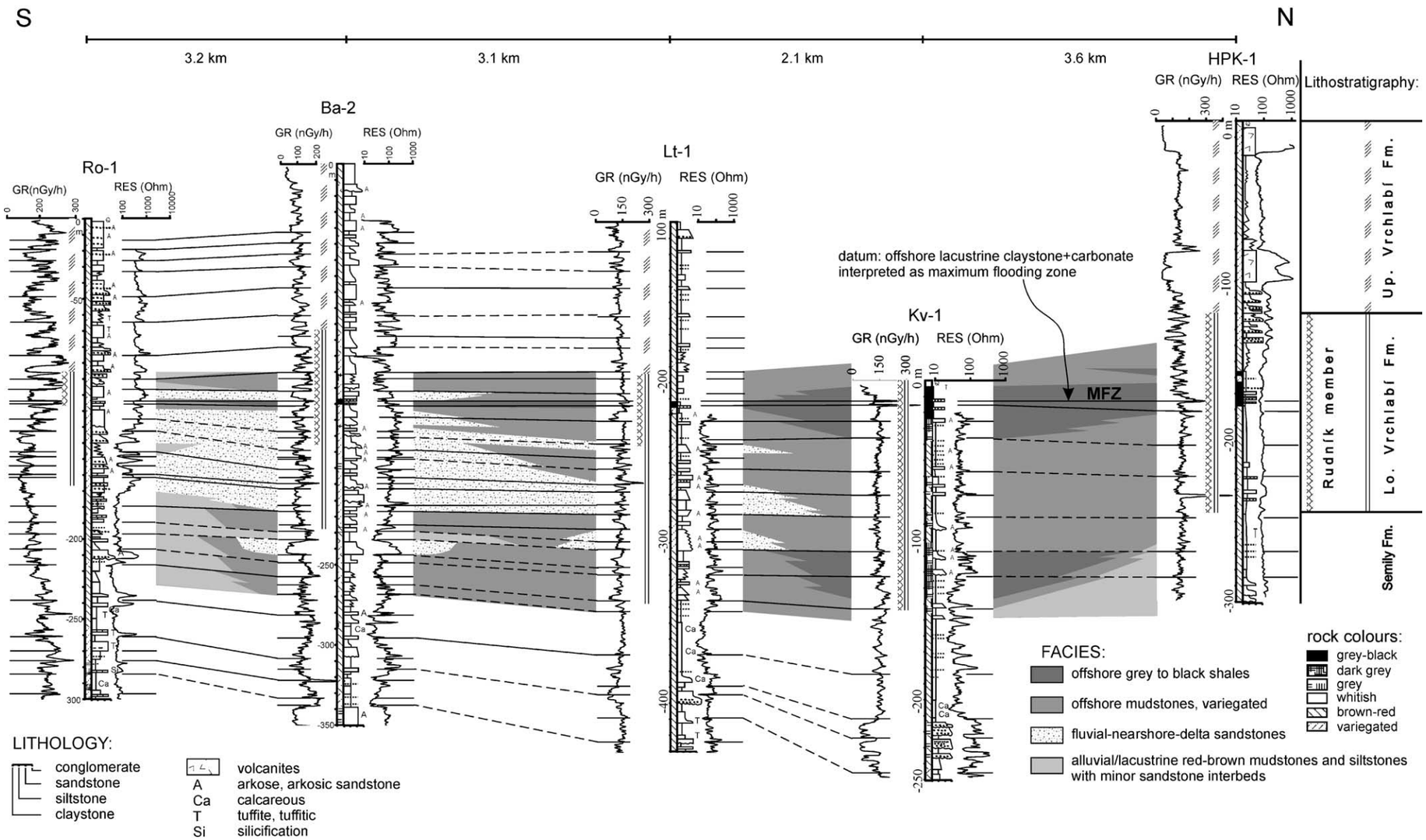

Fig. 3. Cross-section of the Lower Vrchlabí Formation, showing asymmetry of the basin fill during the accumulation of Rudník Lake deposits. The datum used is an interpreted maximum flooding surface (MFS) associated with black shale and a carbonate bed with very high TOC content (up to 23%) in the central part of the basin. This can be correlated to the south to grey lacustrine mudstone and carbonate beds. Generalized sedimentary facies transitions are shown for Rudník Lake deposits only. f — highly faulted and jointed rocks. The high gamma peak in HPK-1 234 m is ascribed to a volcanogenic admixture. Horizontal distances not to scale; for location of boreholes see Fig.1.

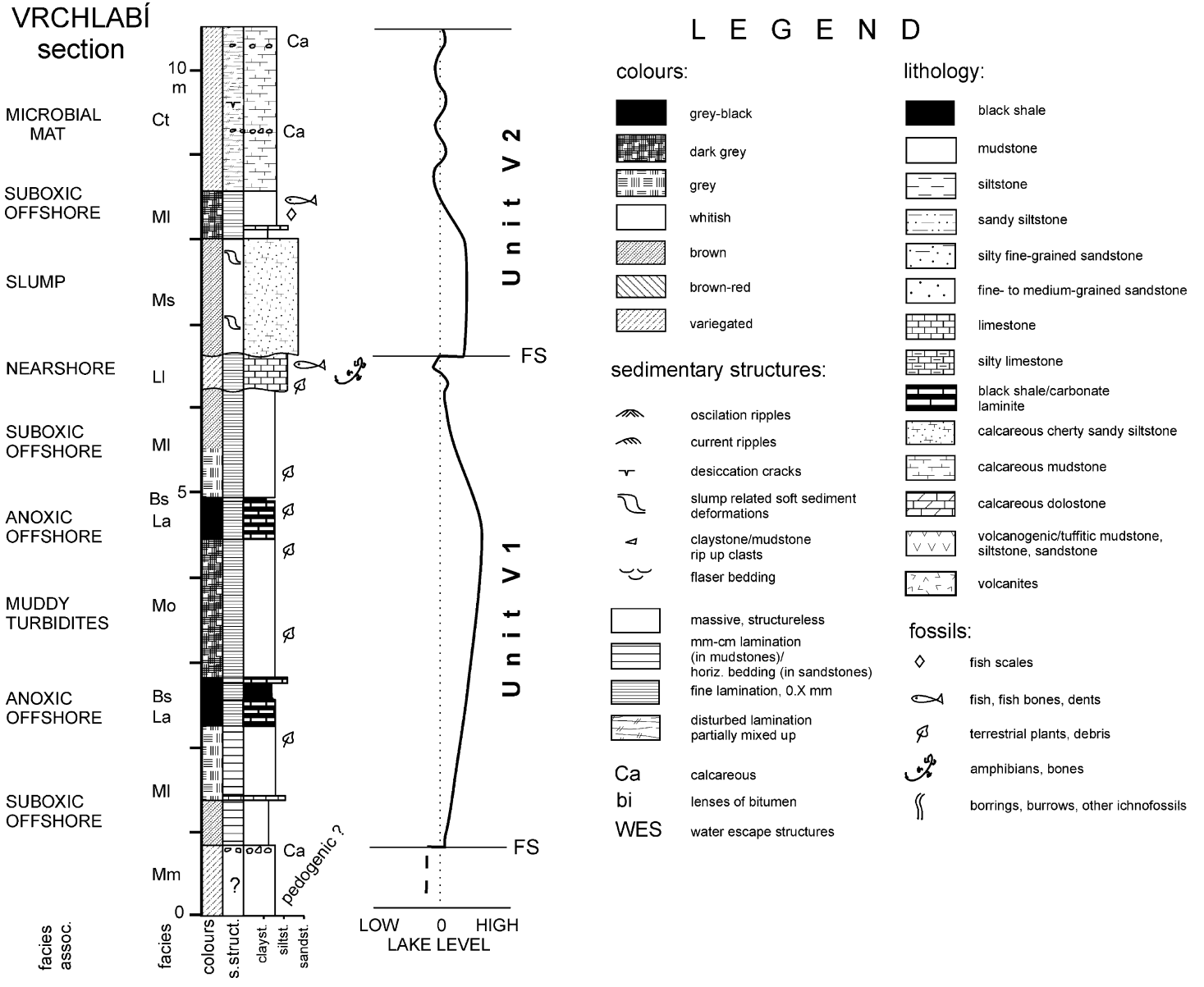

Fig. 4. Sedimentological section measured at Vrchlabí, sedimentary facies (Table 1), facies subassociations and interpreted lake-level changes are shown.

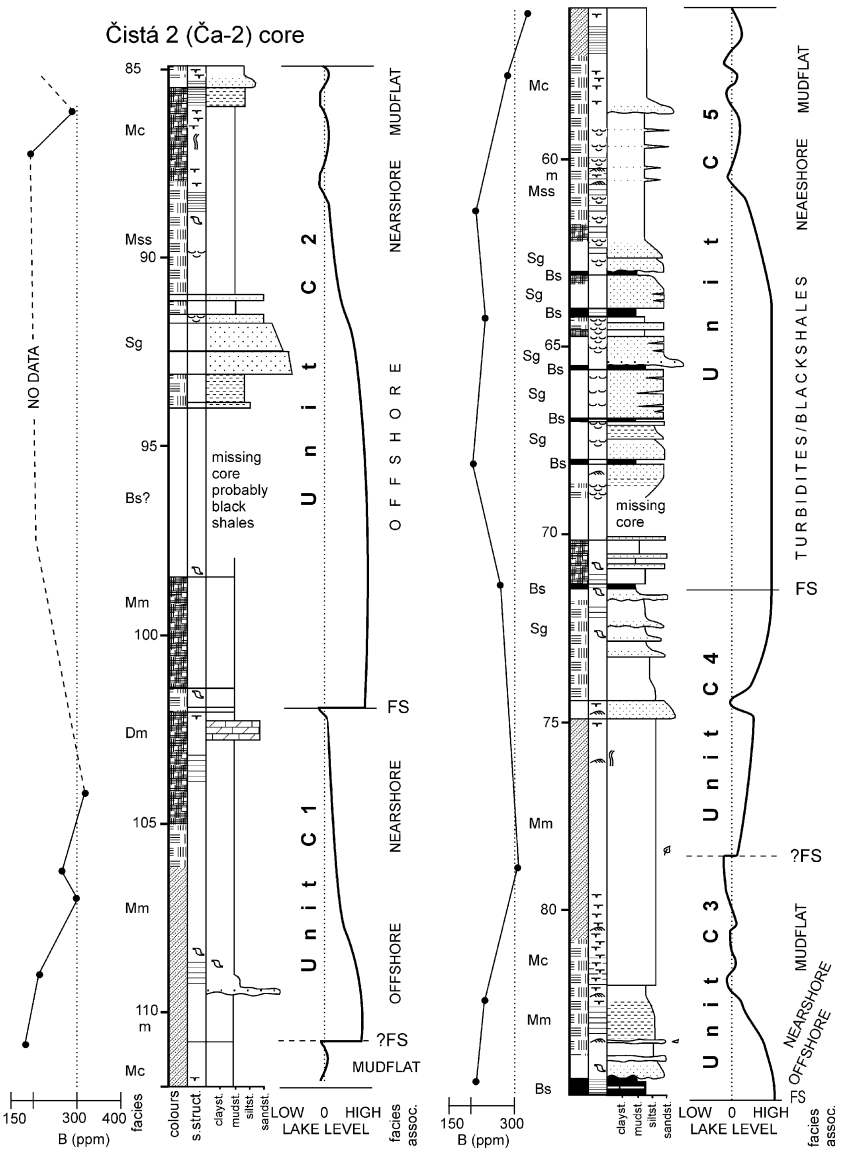

Fig. 5. Sedimentological section measured in well core Čistá 2 (Ča-2), sedimentary facies (Table 1), facies subassociations and interpreted lake-level changes are shown. For legend see Fig. 4.

documentation of core material (Fig. 3). The use of geophysical logs, enabled the lacustrine offshore and nearshore facies and fluvial facies to be correlated.

3.2. Well-log correlation and basin-scale facies architecture

In order to document a basin-scale stratigraphic architecture, relevant for understanding the detailed sedimentological aspects, a N–S cross-section showing correlation of well-log and core data is presented (Fig. 3; for location of boreholes see Fig. 1). The well-log correlation in Fig. 3 represents a transect across a range of depositional systems that form the Semily and Vrchlabí Formations. The general decrease in grain size towards the north is interpreted as a transition from fluvial and deltaic-dominated palaeoenvironments in the south to lacustrine offshore-dominated

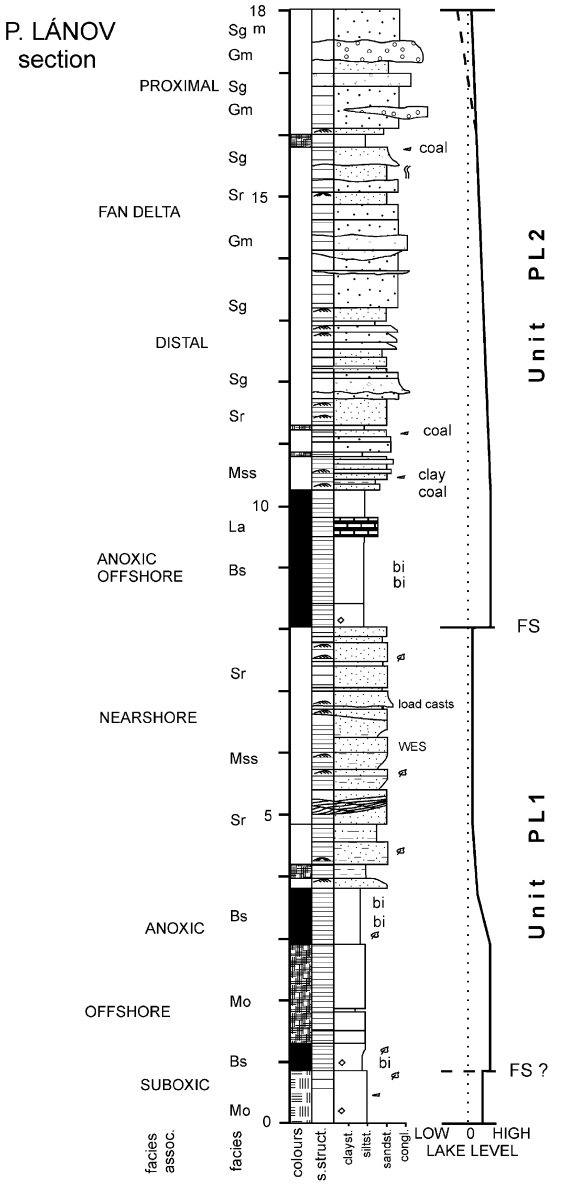

Fig. 6. Sedimentological section measured at Prostřední Lánov, sedimentary facies (Table 1), facies subassociations and interpreted lake-level changes are shown. For legend see Fig. 4.

palaeoenvironments in the north (cf. Prouza and Tásler, 2001). Schematic lithological variations and facies interfingering are shown only for the uppermost part of the Semily Formation and lower part of the Vrchlabí Formation (Fig. 3).

The well-log patterns are dominated, especially in the upper parts (e.g., Fig. 3), by a serrated pattern typical of alluvial/delta plain and some lacustrine deposits (cf. Rider, 1996; Posamentier and Allen, 1999), with occasional blocky log motifs corresponding to sand-dominated alluvial channels (especially logs Ro-1, Ba-2). Maxima in the gamma-ray curves and minima in the resistivity curves correspond to maximum mud contents, as confirmed by core documentation. Vertical variations in sand and mud content become more apparently cyclical further down in the logs, where a repetitive bow-like log motif becomes typical in places in the Semily Formation (e.g., Ro-1100-200 m, Ba-2100-300 m). In the mud-dominated, lacustrine facies of the northern part of the cross-section, only occasional intercalations of sandy strata occur.

The correlations of well-logs across several tens of kilometres are based on the application of the accommodation/supply (A/S) ratio concept (Martinsen et al., 1999). The lithological variations reflected in the varying sand/mud content show similarities for boreholes spaced several kilometres apart, and are interpreted here as a response to cyclical changes in the ratio between accommodation and clastic supply, reflected in both the fluvial-dominated system in the south and the linked lacustrine system in the north. Pronounced maxima in gamma-ray curves are interpreted as flooding surfaces in the lacustrine system, corresponding to expansion surfaces in the coeval alluvial plain (cf. Martinsen et al., 1999). Maxima probably represent a response to a relative rise of lake level in the lacustrine (borehole Kv-1 and Lt-1) and deltaic (Ba-2) settings, accompanied by the expansion of the lake and consequently retrogradation of coarser-grained facies (cf. Sweet, 1999). Similar well-log curve patterns can also be observed in borehole Ro-1 in the red-brown sandstones and mudstones, interpreted as predominantly fluvial facies (Fig. 3). The higher mud contents in some intervals can be explained by lower topographic gradients and lower stream energy during the base level rise. An interpreted maximum flooding surface (MFS) of the Rudník Lake succession lies at the base of a significant black shale and carbonate bed with very high TOC content (up to 23%) and is used as a correlation datum (Fig. 3). The MFS correlates to the south with the base of a grey lacustrine mudstone and carbonate bed (borehole Ro-1). The flooding surfaces are commonly sharply overlain by fining-

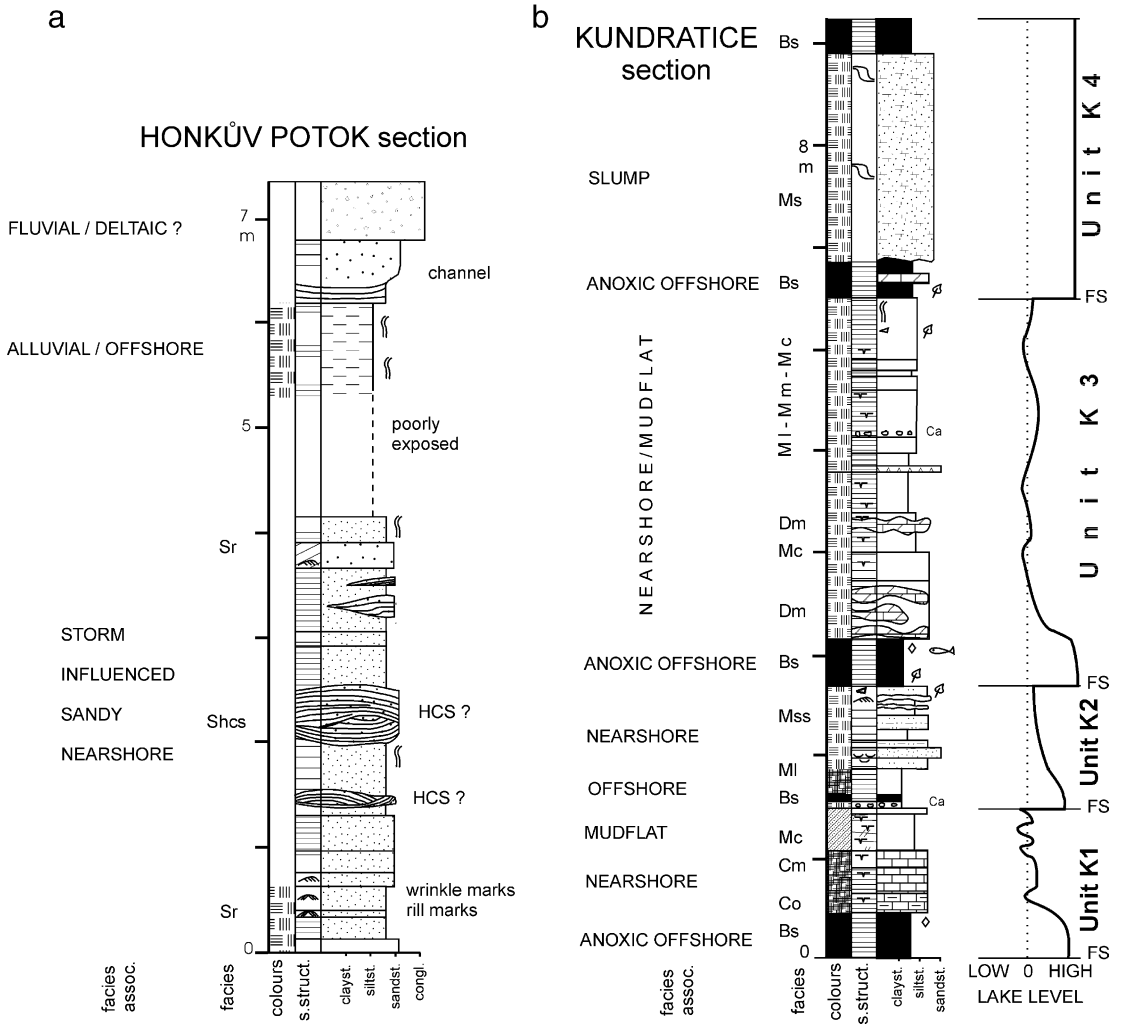

Fig. 7. Sedimentological sections measured at a) Honkův Potok and b) Kundratice localities, sedimentary facies (Table 1), facies subassociations and interpreted lake-level changes are shown. For legend see Fig. 4, for detailed description see text.

upward, coarser clastic successions. This feature can be seen in both distal and proximal delta/lacustrine facies as well as in fluvial facies. Consequently such an incision is interpreted as being connected with an abrupt relative drop of lake-level followed by a gradual rise of lake-level. Similar interpretations, although with slightly different terminology, are presented from the Eromanga Basin, Australia (Posamentier and Allen, 1999, their Figs. 4.25 and 4.69), from Newark Basin (Olsen, 1986; Schlische, 1992, 1993) or from East Greenland (Dam and Surlyk, 1993).

The syn-depositional basin geometry can be interpreted, taking into account the significant differences in pre-compaction thickness of the facies present (Fig. 3). The post-compaction thickness of the Rudník Lake succession increases from 130 m in the south (Ro-1) to at least 150 m in central part of the basin (Kv-1). In the northern part of the basin it may reach 300 m, as reported by Prouza and Tásler (2001), although direct evidence from subsurface data is missing in this part of the basin. Using decompaction equations (Allen and Allen, 1990) and the porosity coefficients of Sclater and Christie (1980), the difference in pre-

compaction thickness was estimated, with input data as follows: 70% of sandstone, 30% of mudstone in Ro-1 and 90% of mudstone and 10% of sandstone lithologies in Kv-1 borehole. An overburden of 1 km of younger deposits is considered although this may be underestimated. Based on these assumptions, an approximate pre-compaction thickness of Ro-1 of 186 m and Kv-1 of 255 m was calculated, representing an increase towards the north of 37%. This significant increase in thickness towards the main boundary fault and the basin-fill style suggests an original half-graben morphology for the basin (e.g., Gawthorpe et al., 1994; Gawthorpe and Leeder, 2000).

3.3. Sedimentary facies

3.3.1. Facies and facies associations

A total of 17 sedimentary facies are recognised within the Rudník Lake deposits on the basis of the lithology, colour, sedimentary and biogenic structures, mineral composition and total organic matter content. These facies record specific sedimentary depositional processes, interpreted from the hydrodynamic and biogeochemical point of view (Table 1). The sedimentary facies are grouped into four facies associations interpreted as: A) anoxic offshore, B) suboxic to oxic offshore, C) nearshore and mudflat and D) slope deposits. Their main descriptive features and interpretations are briefly summarized below.

3.3.1.1. Facies association A — anoxic offshore. The anoxic offshore facies association is composed of black shales (facies Bs, Fig. 8a, Table 1), grey to black mudstones (facies Mo — pelagic unit, Fig. 8d) and carbonate/black shale laminites (facies La), which are characterised by fine laminations, a high organic matter content and a lack of bioturbation. Alternating 1) dark, organic rich laminae and clay minerals with low carbonate content and 2) light laminae rich in carbonate and with lower organic matter and clay content usually form lamination. Fish fossils, amphibians and terrestrial flora can also be present.

3.3.1.2. Facies association B — suboxic to oxic offshore. Finely laminated grey, variegated, to red-brown mudstones and carbonates with low or no organic matter content form facies association B in which bioturbation, amphibians and terrestrial flora can be present. Facies association B comprises laminated mudstone (Ml, Fig. 9b) and laminated limestone (Ll) facies (Table 1).

3.3.1.3. Facies association C — nearshore and mudflat. Facies association C comprises seven carbonate and siliciclastic facies, mostly red-brown in colour: Cm, Ct, Dm (Fig. 9a), Mm, Mss, Sr and Shcs (Table 1). The main characteristics are the presence of desiccation cracks, bioturbation, current and oscillation ripples. The evidence of oscillatory and traction currents indicate shallow water and/or nearshore conditions. The mudflat facies, Mc, comprises mudstones with evidence of repeated desiccation and flooding such as abundant desiccation cracks, pedogenic carbonate nodules.

3.3.1.4. Facies association D — slope deposits. Facies association D is characterised by sharp- to erosionally-based beds of siltstones, sandstones and conglomerates showing slump, graded or massive structures and, rarely, tool marks at the base of beds. Facies Ms, Sg (Fig. 8e), Gm and Mo (silty unit, Fig. 8d) are interpreted as products of turbidites, debris flows and slumps deposited offshore on the lake slope.

3.3.2. Vertical facies pattern and environmental interpretation

Particular sedimentary facies and facies associations form different stacking patterns in different lateral basin settings. Typical sections are presented in Figs. 4–7, each representing a particular part of the lacustrine sedimentary systems interpreted as: 1) the offshore mudstone-dominated central part of the lake; 2) sandstone turbidites; 3) fan-delta; 4) sandy nearshore; 5) mudstone-dominated low-gradient lake margin. The studied sections record lacustrine sedimentation of the upper black shale unit of the Rudník member closely associated with bituminous carbonates (0 to −40 m in Kv-1 on Fig. 3; the lower black shale unit, −100 to −140 m in Kv-1, is not exposed).

3.3.2.1. Vrchlabí section: offshore black shales and laminites. The Vrchlabí road-cut is situated on the present northern basin margin (Fig. 1), where a monotonous 130 m thick succession of dark-grey to black

Table 1
Sedimentary facies of the Rudník Lake deposits

Facies	Colour, lithology, structures, mineralogy	Biogenic structures, fossils, TOC, X-Ray	Interpretation
Mudstone facies			
Black shale Bs	Black to grey-black finely laminated (0.2 to 2 mm) organic matter very rich claystones and silty claystones; 0.1 to 0.5 m thick beds low carbonate content (0–5% normally, 30% max.), mostly calcite mm thick lenses of bitumen can be present as well as bitumen filling tectonic fractures; interbedded carbonate layers 0.5–10 cm thick pyrite on bedding planes in places; Fig. 8a, b	5–23% TOC fish scales, bones, fish fossils; terrestrial plant fragments Q, F>I, K>C, D, A, H C>F, H, D, I, Q, C>D, F, Q>I, K, H calcite dominated carbonate fraction	Sedimentation from suspension anoxic bottom high bioproductivity ± seasonal lamination (Fig. 8 a, b) *offshore*
Organic-rich mudstone Mo	Dark-grey to black-grey; dolomitic organic matter rich laminated mudstones; mm to cm lamination; 0.1 m to 9 m thick beds pyrite on bedding planes in places; rhythmic alternation of mm to 5 cm thick units of clay mudstone and silty mudstone to siltstone units clay mudstone unit is formed by 0.2–2 mm thick laminae composed mainly of dolomicrospar, clay, organic matter; lamination: alternating laminae rich by dolomicrospar or organic matter and clay minerals; silty unit is formed by one or several amalgamated laminae; main components are : dolosparite, highly corroded quartz silt grains, carbonate intraclasts (micritic or microsparitic, silt sized); two types of silty laminae are present: 1) sharp-based with graded bedding or massive and with gradual top contact, and 2) with gradual transition at the base as well as at the top; see Fig. 8d	Usually 1–4% TOC terrestrial plants, plant fragments D>>Q, I, F, F>D>I, Q, H D>F>I, H, Q entirely dolomitic, no calcite found	Anoxic bottom high bioproductivity clay mudstone unit: sedimentation from suspension silty unit: underflows and interflows *offshore*
Laminated mudstone Ml	Grey, variegated, brown; laminated dolomitic or calcareous mudstones mm to cm lamination; 0.1–1.5 m thick beds; different proportion of clay, silt, organic matter and carbonate in particular laminae; 5–10 mm thick silty laminae occur in places usually sharp-based and graded bedding in places	Max. 0.2–1% TOC; terrestrial plants, plant fragments; coprolites, fish fossils bioturbation can be present D, F>C>I, K, Q D>>F>Q, I, C, K both dolomite as well as calcite can be present	Suboxic bottom sedimentation from suspension with occasional underflows (gravity flows); lamination can be driven either by climate or by sediment supply *offshore*
Mudcracked mudstone Mc	Red-brown, brown, grey calcareous mudstone 0.1 m to several metres thick beds; cm or disturbed lamination or massive; abundant mudcracks disturb original lamination; pedogenic mottling and claystone rip up clasts can be present; cm to 0.5 m interbeds of heterolithic clayey silty sandstones with rare mudcracks in some places	0.2–1% TOC can be present; plant fragments in some places; (Kundratice section: C, Q, A>I, D>F, K; Q, C, A>I, F, H, K; Q, C>I, D>K, F, H calcite dominated carbonate fraction)	Frequent alternations of flooding periods with sedimentation from suspension and desiccation with subaerial exposure; *mudflat*
Mottled mudstone Mm	Red-brown, brown, grey-brown, grey calcareous mudstones to siltstones 0.2 m to several metres thick beds pedogenic mottling, mixed up clayey/silty material or crude lamination in some places; rare lensy bedding with silty lenses	Bioturbation can be present	Primary possibly laminated structures disturbed by later processes–pedogenesis, bioturbation *nearshore/alluvial plain*
Carbonate facies			
Carbonate/black shale laminite La	Carbonate and organic matter rich mudstone laminite; 0.2–2 mm thick laminae; alternating of 3 types of laminae: 1) micritic organic matter rich mudstone laminae, grey; 2) organic matter very rich mudstone laminae, black; 3) pure microspar laminae with dispersed organic matter, whitish, silty Q grains can be present microspar laminae are lensy in some places; 1–2 cm nodules of bitumen can be present; 0.1–0.5 m thick beds	2–12% TOC plant detritus high carbonate content—approx. 50% D>F>C>I, Q, H D>>>F, C, A C>F, D>I dolomite as well as calcite are present	Sedimentation from suspension anoxic bottom seasonal bioinduced carbonate precipitation high bioproductivity *offshore*

Organic-rich carbonate Co	Grey to dark-grey laminated limestones and dolomitic limestones; 0.5 m thick bed; organic matter rich; clayey microspar (Fe calcite and Fe dolomite); dark and light laminae with different proportion of organic matter, clay and carbonate content; low lithological contrast between dark and light laminae; lower part with higher organic matter content is finely laminated — 0.2–2 mm; upper part with lower organic matter content have millimeter-scale lamination; highly corroded silt quartz grains or peloids can be present occasionally	0.3–8% TOC high carbonate content — 50–70%	Anoxic to suboxic bottom increasing upwards carbonate precipitation rate high bioproductivity *offshore*
Massive (organic-rich) carbonate Cm	Grey to dark grey massive carbonate 20 cm thick bed; microspar to sparry with relics of clayey micrite matrix; micrite peloids (up to 30%) or highly corroded silt quartz grains can be present; organic matter in the form of dispersed opaque grains; mudcracks on the top		Shallow water carbonate precipitation high bioproductivity *nearshore*
Laminated limestone Ll	Violet-red laminated limestone; 0.5 m thick bed; fine lamination: 0.2–2 mm; dark laminae: clayey microspar with dispersed organic matter or Fe pigment; light laminae: pure microspar to sparite; clayey organic matter rich laminae in some places; rare peloids	Fish and amphibian fossils, coprolites, terrestrial plants	Suboxic to oxic bottom high bioproductivity lamination probably seasonal *nearshore* (low energy)
Muddy dolostone Dm	Grey muddy limy dolostone; cm to 0.5 m thick lensy or nodular beds, massive to concentric zonal fabric (higher carbonate content in the centre, higher organic matter content in outer rim); clayey dolomicrospar, silty quartz grains admixture, dispersed opaque grains of organic matter; mudcracks on top bedding plane in some places; secondary porosity filled by drusy and blocky sparite calcite cement; Figs. 9a,b	D>>Q>F, C, I	1) Shallow water carbonate precipitation; palustrine; *nearshore* 2) precipitation from saline lake water— Coorong model; *nearshore*
Carbonate microbial mat Ct	Grey green, grey violet, grey red, mottled; laminated muddy carbonate undulose lamination (Fig. 9c); alternation of clayey microspar laminae with laminae rich in partly oxidised organic matter; lamination is often disturbed, mixed up material, mudcracks in some places; horizons of cm-sized calcareous nodules		Shallow water precipitation and sedimentation on microbial mats; followed by subaerial exposure and pedogenesis *nearshore*
Sandstone/conglomerate facies			
Mudstone, siltstone and sandstone interlamination Mss	Red-brown to grey alternation of mm to cm laminae of mudstone, siltstone and fine-grained sandstone; proportion of particular laminae is highly variable transition of lamination to lensy or flaser bedding can be present heterolithic, carbonatic fine to coarse-grained sandstone interbeds 3–10 cm thick, massive or rippled or flaser bedded, good to poorly sorted; occasionally with plant debris, mudstone or coal intraclasts and mudcracks	Bioturbation in some mudstone-rich horizons (Kundratice: D, Q, F>I, K, C)	Higher siliciclastic input alternation of different hydrodynamical regimes shallow water (where desiccation cracks are present) *nearshore* (mud to sand flats) to distal prograding sand bodies
Sandy mudstone Ms	Greenish-grey to reddish; sandy limy silicified mudstone; clayey (zeolites ?) matrix with microspar, quartz silt and fine-grained sand grains, diffused opaque grains of organic matter; volcanogenic material (angular quartz grains with fluid inclusions, felsitic grains); 1–2 m thick beds, thickness laterally highly variable; slump structures, plastic deformations or massive, sharp to erosional base; claystone intraclasts and plastically deformed underlying mudstone rip up clasts (facies Bs or Ml) near the base; Fig. 8.c)		Rapid sedimentation probably driven by volcanic activity: volcanogenic fall and seismic activity (Semily volcanic centre is 10 to 25 km away) slump *offshore*, lake slope
Rippled sandstone Sr	Grey, whitish; fine to medium-grained sandstones; 0.1–0.6 m thick beds horizontal bedded, laminated, isolated ripples, rarely oscillation ripples medium to well sorted, well rounded; thicker beds can be amalgamated and show planar or trough cross bedding	Plant fragments or bioturbation in some places	Sedimentation from traction and/or oscillation currents

(continued on next page)

Table 1 (*continued*)

Facies	Colour, lithology, structures, mineralogy	Biogenic structures, fossils, TOC, X-Ray	Interpretation
Sandstone/conglomerate facies			
Hummocky cross stratified sandstone Shcs	Grey, whitish; medium-grained sandstone; 0.1–0.5 m thick lensy beds; sharp base and top; well sorted; form interbeds within sandstones of Sr facies; hummocky cross stratification		Sedimentation from storm currents and waves
Graded and massive sandstone Sg	Grey, whitish; fine to coarse grained sandstones; 5 cm to 0.7 m thick beds poorly to moderately sorted; sharp or erosional based; rarely with flute casts and groove marks on the base; coarse to medium grained sandstones with graded bedding often overlain by fine-grained sandstones with ripples, flaser and lensy bedding (gradually passing up to the grey mudstones); sometimes massive with no graded bedding; beds could be also amalgamated or alternate with black shales (Bs facies)		Deposits of turbidity currents
Matrix-supported conglomerate Gm	Fine-grained conglomerates (mm pebbles, max. 3 cm), rarely medium; grained (cm pebbles, max. 20 cm); 0.2–0.4 m thick beds; massive, matrix supported; subangular to well rounded pebbles; medium to coarse grained clayey sandstone matrix; two types: 1) tabular beds, sharp planar base, planar or undulose top; 2) lensy trough-like beds with erosional base		1) Cohesive debris flow 2) non-cohesive debris flow

Symbols used for mineralogical composition obtained by X-Ray diffraction: C — calcite, D — dolomite, Q — quartz, A — analcite, I — illite, F — feldspars (both K- and Ca-feldspars are present), K — kaolinite, H — hematite; D > C means that dolomite content is significantly higher than calcite content; C >> D means that calcite content is much higher than dolomite content; C, D means that calcite content is of similar percentage than dolomite content; minerals are sorted from left to right by decreasing content in the sample; relative portion of individual minerals in the sample was obtained by comparing the three highest peaks in the X-Ray difractogram; detection limit is approximately 5% of mineral phase in the sample. All X-Ray diffraction data are from Kundratice and Vrchlabí sections only. TOC — total organic carbon.

laminated mudstones with rare intercalations of black shales and carbonates crops out (Drábková et al., 1990). The determination of thickness is only approximate, because the outcrop is deformed by several small thrust faults. The section (corresponding to Section 4 of Drábková et al., 1990) represents only a small part of this outcrop, but is the most diverse lithologically: offshore anoxic black shales and laminites are present as well as shallow-water carbonates and microbial mat deposits.

Two distinctive units are recognised (Fig. 4). At the base of the section, mottled mudstones with carbonate nodules of probably pedogenic origin occur. The interpretation of these mudstones remains problematic, because the original structures are disturbed by jointing and fluid migration along a nearby fault. The base of the overlying Unit V1 is marked by a flooding surface at the base of finely laminated offshore mudstones of facies Ml. These mudstones show a gradual upward increase of organic matter content, accompanied by a gradual decrease in iron oxides, reflected by a gradual change of colour from red-brown at the base through grey-brown to dark grey at the top. These trends are interpreted as a record of the lake bottom waters' increasing oxygen depletion, which could be caused by a rise of lake level and the establishment of a stratified water column as well as by an increase in bioproductivity. The overlying anoxic offshore facies Bs, La and Mo probably represent the period of highest lake level with permanent stratification and high bioproductivity. Beds characterised by alternations of well-defined black clayey laminae and white microspar laminae (similar to the anoxic facies of the Kundratice section, Fig. 7 b) are common within this succession and are interpreted as reflecting seasonal variations of bioproductivity, sediment input and water chemistry. Mudstones of facies Mo containing rhythmic alternations of pelagic mudstone laminae and silty laminae (Table 1, Fig. 8d) are interpreted as products of occasional underflows and interflows triggered by hyperpycnal inflows. No periodicity was found in the thickness of both types of packets. They could have been driven by seismicity caused by tectonic activity on the northern marginal basin fault zone. The presence of turbidity underflows can indicate a higher topographic gradient along the northern basin margin. A gradual upward decrease in organic matter content and increase of iron oxides within the overlying offshore facies Ml is interpreted to record an increase in lake bottom oxygenation, which may be caused by a drop in lake level. Alternatively oxygenation of deep water can be caused by water mixing, which is primarily controlled by surface wind stress in deep tropical lakes. Thus apparent fluctuations in bottom-water oxygen supply could also be a result of changes in wind intensity. The top of unit V1 is a finely laminated nearshore carbonate Ll, which is characterised by alternations of dark grey, organic matter-rich laminae and red-violet iron oxides pigmented submilimetre-thick laminae. This unusual feature can be caused by seasonal/annual changes of bioproductivity and a relatively high carbonate accumulation. Rapid precipitation of carbonate could prevent black shale laminae oxygenation during later oxic conditions. The presence of amphibian fossils provides evidence of relatively shallow water conditions. The lower part of the overlying Unit V2 is formed by a sandy mudstone slump bed (Ms) overlain by anoxic to suboxic offshore mudstones Ml. The upper part of unit V2 is formed by muddy microbial mat carbonate with mudcracks and pedogenic nodules at the top. Slump and anoxic offshore facies are interpreted as a record of a significant rise in lake level and lake highstand, where a subsequent drop in lake level is indicated by the overlying microbial mat facies.

The absence of coarser clastic deposits, even in nearshore facies, implies a relatively low sediment input, suggesting that the Vrchlabí section was located near the depocentre. In this case substantial changes in lake level, causing large lateral shifts of coastline, seem to be necessary in order to explain the vertical facies transitions from anoxic offshore black shales and distal silty turbidites to shallow water carbonates or microbial mats (Dam and Surlyk, 1993).

3.3.2.2. Čistá 2 section: deepwater turbidite fans. The Čistá 2 section comes from a well core from the north-eastern part of the basin (Fig. 1). Lower boron values are interpreted as sedimentation in more freshwater conditions at times of high lake level, in contrast to higher boron values, which are interpreted as sedimentation in more saline conditions during low lake level (Blecha et al., 1999).

The lower part of the well core mainly represents lacustrine deposits of the Rudník member (Fig. 5).

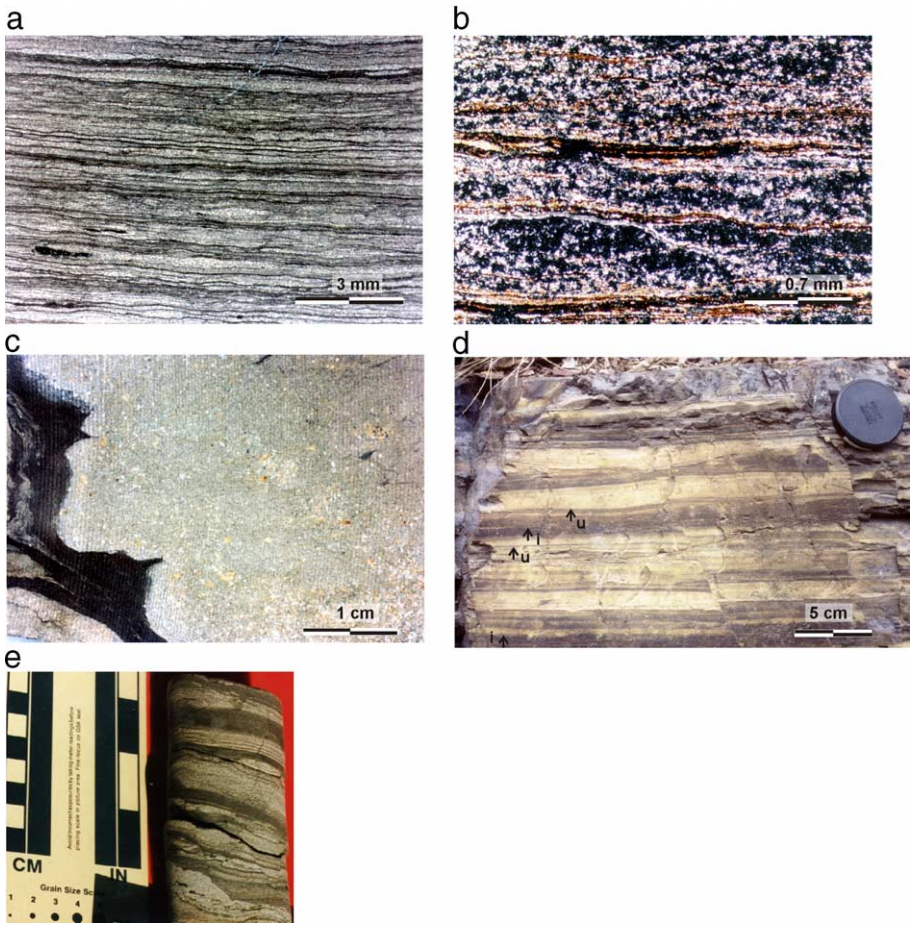

Fig. 8. a) Even lamination of black shale facies (Bs). Most of the rock is composed of clay minerals, black laminae are rich in organic matter, which is interpreted as having been deposited during annual/seasonal algal blooms. Whitish lenses and lensy laminae are composed mainly of clay minerals and microspar crystals of early diagenetic origin; black lenses (lower left) are later diagenetic bitumen lenses. Kundratice section, 0.2 m, rock slab, reflected light. b) Close-up view showing even algal laminae (brown) and mixture of kaolinite, illite and analcite (grey to black) and microspar crystals (bright) scattered in a clay mineral matrix. Transmitted light, crossed nicols. c) Base of the slump bed (facies Ms) showing large plastically deformed laminated black shale rip up clast (black), smaller grey mudstone rip up clast and pale yellow intraclasts of probable volcanogenic origin. Kundratice section, 6.9 m, rock slab, reflected light. d) Outcrop showing facies Mo in Vrchlabí section 3.5 m. Sharp-to erosional-based normally graded silty laminae of distal turbidity underflows and sharp-to diffuse-based silty laminae of interflows can be seen. Lens cap is 5 cm in diameter. e) Čistá 2 well core showing alternation of mm – cm laminae of black shales (Bs) and turbidite sandstones (Sg). Small-scale faults can also be seen in the lower part. Ča-2, 67.30 m.

The overlying succession is mainly formed of red-brown mudstones of alluvial/ephemeral lake origin. It contains millimetre–centimetre thick intercalations of early diagenetic displacive gypsum, indicating hydrologically closed basin conditions and high water output/input ratio.

Based on flooding surfaces, located at the base of laminated offshore lacustrine facies (e.g., black shale) intervals, the section can be divided into five units (Fig. 5). The lower 3 units, unit C1, C2 and C3 show a distinctive shallowing-up pattern. The lower part of these units is usually formed by offshore mudstone facies Mm and Bs; the Mm facies is interpreted here as offshore, because of low boron values (Fig. 5). Massive or graded sandstones of Sg facies are also present. Alternation of millimetre-centimetre laminae of black shales and turbidite sandstones is a very common feature (Fig. 8e). Nearshore Mss and Dm

facies, or Mm facies with higher boron values overlie these beds. Mudflat Mc facies can be present on the top of units. The recognition of a flooding surface between units C3 and C4 is problematic, because the massive mudstone facies Mm of the lower part of unit C4 can be interpreted as deposited on an alluvial plain as well as in a lacustrine environment. In addition, no sharp surface or lithological boundary was observed. The overlying succession of the Mm and Sg facies probably records occasional turbiditic sedimentation during a rise in lake level. Unit C5 is also a shallowing-up unit, but is distinguished from units C1-3 by a thick offshore succession dominated by turbidite sandstones with minor black shales in the lower part. Nearshore Mss facies and mudflat Mc mudstones form the upper part of the unit. The presence of a relatively thick sandstone turbidite succession can provide evidence of a nearby high gradient basin margin and can be interpreted as part of a deep-water turbidite fan. Alternatively the turbidites could have been generated from a large delta built by a river entering the lake from an axial or flexural margin direction (cf. L. Tanganyika, Tiercelin and Mondeguer, 1991; Huc et al., 1990).

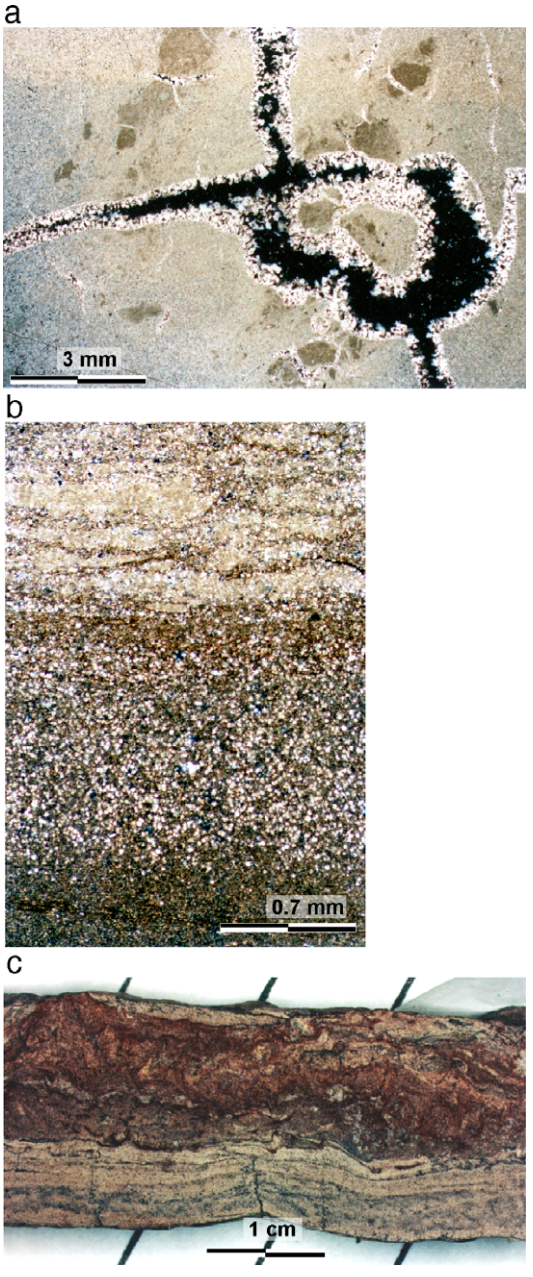

Fig. 9. a) Secondary porosity developed in muddy dolomite facies (Dm) showing drusy calcite cement fringe (bright) and later analcite infill (black). Kundratice section, 3.6 m, transmitted light, crossed nicols. b) Gradual transition between organic-rich laminated mudstone (facies Ml, at the base) and muddy dolomite (Dm, at the top). Transitional unit (Tr, in the middle), originally facies Ml, is modified by early dolomitization, euhedral to subhedral small dolomite crystals (bright) are abundant. Kundratice section, 3.6 m, transmitted light, crossed nicols. c) Microbial mat with well-preserved undulose laminated grey lower part and oxidised, probably pedogenically disturbed red-brown upper part. Vrchlabí section, 10.1 m, polished rock slab.

3.3.2.3. Prostřední Lánov section: fan-delta system. The Prostřední Lánov section is situated near the present northern basin margin (Fig. 1).The section can be divided in two distinctive shallowing-up units, which are separated by a flooding surface (FS, Fig. 6). Unit PL1 is characterised by a transition from offshore anoxic facies Mo and Bs at the base towards nearshore siltstone and sandstone facies Sr and Mss (Table 1). Current ripples show climbing, and oscillation ripples, load casts, ball and pillow and water escape structures are also present. The latter facies indicate rapid sedimentation from traction and oscillation currents, which is typical for nearshore sand bodies. They probably represent nearshore bars and sand bodies and their progradation was most likely due to a drop of lake level. The top of unit PL1 is overlain by anoxic offshore facies Bs and La, which form the base of unit PL2 and is interpreted as the result of a significant rise of

lake level. The upper part of unit PL2 is interpreted as progradation of the sandstone and conglomerate bodies. The lower part of the succession is characterised by progradation of Mss, Sg and Sr facies, which are characterised by sharp bases and graded bedding. They are traction and turbidity current products. This contrasts to the upper part of section, where, in addition to the Sg and Sr facies, Gm conglomerates form a significant portion. Both matrix-supported and clast-supported conglomerates are present and are interpreted as deposits of cohesive and non-cohesive debris flows, respectively. The evidence for rapid sedimentation and vertical facies succession supports the interpretation of a fan-delta system. The lower part of the fine-grained sandy turbiditic unit PL2 probably represents distal fan-delta deposits, conglomeratic debris flows are interpreted as having been deposited on the proximal part of a fan-delta. There are no indicators of water depth in this part of the section, so it is not clear whether sedimentation took place in a subaqueous or a subaerial part of the fan-delta (Sneh, 1979).

3.3.2.4. Honkův Potok section: sandy nearshore. The section of Honkův Potok records a relatively short period of lacustrine sedimentation in the northwestern part of the basin (Fig. 7a). The section is located in the small valley of Honkův Potok Creek, where several small and scattered (usually 1–2 metres thick) sections of mainly lacustrine black shales containing lacustrine fauna of the Rudník member occur (Fig. 1).

The lower part of the section is dominated by sandstones of the Sr and Shcs facies (Fig. 7a), interpreted as sedimentation products from traction and oscillatory stream wave currents, storm waves and currents, respectively. Alternation of these facies probably indicate changing water depth with conditions of sedimentation alternating between a near fair-weather wave base and a near storm-weather wave base, which can be interpreted in terms of lake-level fluctuations. Facies Sr, with its small oscillation ripples (5–20 cm wavelength), were probably deposited in much shallower water depths than the overlying Shcs facies with antiforms and synforms (hummocks and swales) with a wavelength of a few metres (Dam and Surlyk, 1993). But alternation of these facies may also be attributed to changes in storm intensity and magnitude.

The upper part of the section is poorly preserved; sedimentary structures and sandstone body geometries have been altered by weathering. Grey laminated and bioturbated siltstones are overlain by flat and trough beds of mostly massive coarse-grained clayey sandstones with a pebble admixture. This part of the section may represent 1) progradation of sand bodies or migration of channels on a delta plain, 2), deposits of a subaqueous delta front setting, and 3) alluvial/fluvial channels and overbank deposits.

3.3.2.5. Kundratice section: mudstone-dominated, low-gradient lake margin. In the Kundratice section, three shallowing-up units were recognised (Figs. 1, 7b). Unit K1 consists of basal anoxic offshore black shales of the Bs facies overlain by an offshore, finely laminated dark grey carbonate bed, which passes up into nearly massive grey mud-cracked nearshore carbonate of the Cm facies. The top of unit K1 is formed by mudcracked mudstones of the mudflat facies, Mc. Unit K1 records lake regression accompanied by carbonate precipitation. Offshore black shales at the base of the unit K2 sharply overlies the mudflat mudstones of unit K1. The base of black shales is interpreted as a flooding surface. Black shales of the Bs facies, representing anoxic offshore sedimentation, are relatively thin and pass gradually into grey laminated mudstones interpreted as having been deposited in more oxygenated offshore sediments. The top of unit K2 is formed by nearshore Mss facies. Unit K3 shows similar features as the underlying units. The basal black shale bed is overlain by a succession of nearshore/mudflat mudstones with interbeds of lenticular, nodular, muddy micritic dolostone beds of the Dm facies. These dolostone facies are interpreted as being precipitated from shallow saline water with the possible influence of fresh groundwater (cf. Muir et al., 1980; Rosen et al., 1989). The dolomites show evidence of subaerial exposure and vadose environments such as mudcracks, secondary porosity, and drusy calcite cement (Table 1, Fig. 9a), and are interpreted as modified or partly formed in a palustrine environment (Freyet and Plaziat, 1982; Platt and Wright, 1992). Unit K4 is incomplete, but consists of rapidly deposited and slumped beds (Ms), possibly of volcanogenic origin, and offshore black shales (Bs).

The absence of coarser clastic material within this section, and the presence of a succession of nearshore/

mudflat facies, up to several metres thick, indicate a low sediment input and low-gradient lacustrine environment. Such environments would be very sensitive to lake-level fluctuations, which were probably the main driving mechanisms producing the facies patterns. Lake-level fluctuations of several orders can be documented. Large lake level rises are marked by four flooding surfaces, minor fluctuations are marked by abundant mudcracks within the nearshore and mudflat facies. The interbedded offshore black shales and mudcracked mudflat facies provide strong support for the changes in relative lake level interpretation discussed below.

3.3.3. Lacustrine calcite and dolomite

Most of the mudstone and carbonate facies contain different proportions of calcite and dolomite. Calcite is present in the form of: 1) micrite or microspar, finely dispersed in mudstone or forming discrete laminae; 2) microspar forming early diagenetic lenses in laminated Bs and La facies; and 3) calcite spar cementing secondary porosity, which is found only in Dm facies. Dolomite is present in the form of dolomicrite and dolomicrospar occurring in the same setting as calcite micrite and microspar. No displacive/replacive textures are found. Grains of detrital dolomite were found within the silty turbiditic laminae of Mo facies. Facies Bs, La, Ml and Dm show changes in dolomite/calcite ratios (Table 1). Black shales of Bs facies are calcite dominated with minor dolomite, while in the muddy dolomites of Dm facies dolomite dominates and the calcite content is very low. Facies La and Ml usually contain significant amounts of calcite as well as dolomite.

Because of the lack of displacive/replacive textures most calcite micrite, microspar, dolomicrite and dolomicrospar was probably precipitated primarily from the lake water or early diagenetically from pore water. Almost all recent lacustrine dolomite is precipitated from saline lake waters with a high Mg/Ca ratio (Last, 1990). Precipitation from pore waters with high Mg/Ca ratio in relatively freshwater lakes is rare. The black shale facies (Bs) with low dolomite content is interpreted as a product of sedimentation/precipitation from the least saline water during high lake levels, in contrast to muddy dolomites of the Dm facies, which needs much more saline water with a higher Mg/Ca ratio to precipitate. These conditions suggest a low lake level. Facies La and Ml, with both dolomite and calcite content, are interpreted as products of sedimentation/precipitation products from moderately saline water during intermediate lake-level. This requires a hydrologically closed lacustrine system with higher salinities during low lake levels and lower salinities during high lake levels. The possibility of early diagenetic dolomitization mediated by organic matter (Slaughter and Hill, 1991) cannot be excluded. Calcite and dolomite of the Bs, La, Mo, Cm, Co and Dm facies are mostly ferroan calcite and ferroan dolomite, which indicates precipitation in reducing conditions.

3.4. Palaeogeography and tectonosedimentary model of the Rudník Lake

Palaeontological evidence suggests that the faunal and floral assemblages of all sections of Rudník Lake deposits belong to one lacustrine period (Blecha et al., 1997; Drábková et al., 1990; Zajíc, 1997; Šimůnek, 1997; Drábková, 1997). Correlation of particular beds between most outcrop sections is not possible because of the large distances between sections (Fig. 1), the high degree of lateral facies variability and postsedimentary deformation of the basin. Only sections situated close to each other can be correlated bed-by-bed. Several black shale dominated outcrops in the Kundratice–Košálov area, not more than a few kilometres apart, contain almost the same sedimentary succession with small variability in the thickness of particular beds. The anoxic offshore facies found in almost all sections of Rudník Lake deposits represent highstand sedimentation in one large lake, which covered an area of at least 400 km^2. During lowstands the lacustrine basin could have been divided into several partly or completely isolated lake sub-basins.

Three areas of distinctive facies development were found (Fig. 10): 1) a central-axial part of the basin dominated by anoxic to suboxic offshore mudstones; 2) the northern basin margin dominated by anoxic black shales and sandy to gravelly gravity currents or nearshore deposits indicating a high gradient basin margin; and 3) the west-central part of the basin dominated by black shales and nearshore facies and mudflats of a low-gradient basin setting.

The presumed lateral distribution of sedimentary environments during deposition of the Rudník member in the Krkonoše Piedmont Basin is shown in Fig.

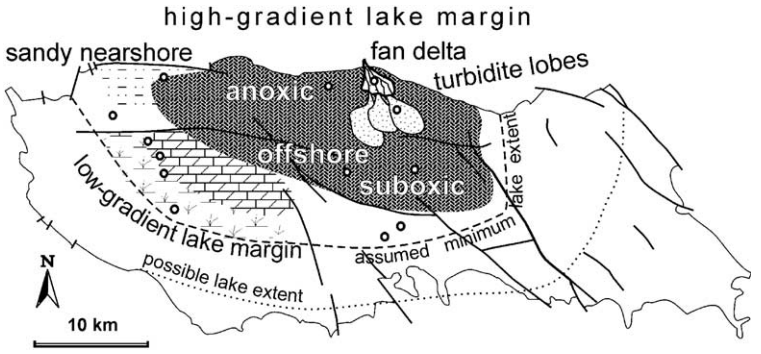

Fig. 10. Simplified palaeogeographical sketch of the Krkonoše Piedmont Basin during the sedimentation of Rudník Lake showing distribution of sedimentary environments. Three palaeogeographic elements are recognised: the anoxic offshore axial basin, a low-gradient mudstone/carbonate dominated southwest margin, and a high-gradient northern margin with gravity driven deposits. Sedimentary environments are placed in the context of the present-day outcropping basin. Circles refer to the studied localities and boreholes (Fig. 1).

10. The central-northern part of the basin, probably representing the deepest, axial part of the basin (Vrchlabí section, borehole HK-1, Fig. 1), contains the thickest succession of anoxic to suboxic offshore facies (Bs, La, Ml). Along the northern basin margin, coarser clastic facies are distributed. Nearshore sandstone facies of the Honkův Potok section probably originated by the redistribution of nearby alluvial fan or fan-delta or fluvial clastic material. These facies could have also been deposited in an accommodation zone between two half-grabens (cf. Gawthorpe and Leeder, 2000) or a hinge zone (sensu Soreghan and Cohen, 1996). The fan-delta system of the Prostřední Lánov section probably supplied the Čistá 2 section's sandstone turbidite bodies. These facies indicate a steep gradient along the northern basin margin. In contrast to this steep-gradient sedimentary system, mainly mudstone/carbonate facies occur in the southwest part of the Rudník Lake. These facies are stacked in several relatively thin, shallowing-up, offshore–nearshore units (section Kundratice in Fig. 7b) and indicate a low-gradient sedimentary system, which was sensitive to lake-level fluctuations. The lateral distribution of sedimentary facies (Fig. 10) and the asymmetry of the basin fill (Fig. 3) allow us to interpret the tectonic setting of the basin during the Asselian as a half-graben. Subsidence along the northern basin margin fault (Fig. 11) was the main driving mechanism determining the sedimentary architecture of the basin fill. Unfortunately, we do not have kinematic indicators to interpret whether the fault was dip-, oblique- or strike-slip. The basin could have developed as a simple half-graben in an extensional regime or as series of transtensional sub-basins along a strike- or oblique-slip fault (Crowell and Link, 1982; Coward, 1986; Scholz, 1995). Because of the limited preservation of nearshore facies along the present-day northern basin margin, we suggest that the main boundary fault was situated northwards of the present-day boundary fault during the Early Permian.

Although no reliable bathymetrical indicators are available, the minimum depth of the Rudník Lake during highstand is interpreted to have been about several tens of metres. This interpretation is based on the presence of lake water stratification indicated by black shales found over an area of 300 km^2 and the thickness of the siliciclastic progradational successions, which need accommodation space to develop. Unit C5 of the Čistá 2 section is thus more than 15 m thick and its original thickness before compaction could have been ca 25 m. The minimal areal extent of a highstand offshore facies of 400 km^2 needs a minimum water depth of several tens of metres to cover topographic highs. Faunal assemblage is relatively diversified. Vertebrates are represented by acanthodians (1 species; Acanthodes), xenacanthid sharks (1 species; Bohemiacanthus), actinopterygians (7 species; Paramblypterus, Amblypterus, Igornichthys), dipnoans (1 species; Sagenodus), amphibians (4 to 5 species; Archegosaurus, Melanerpeton, ?Cheliderpeton, "Ptyonius"), and reptiles (unidentified remains). Invertebrates are represented by pelecypods (?Anthraconaia), conchostracans (Limnestheria, Pseudestheria), ostracods (Carbonita), malacostracans

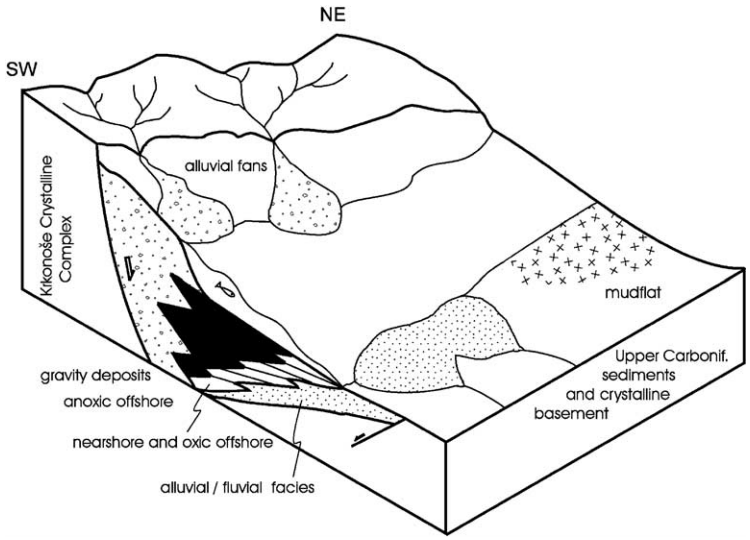

Fig. 11. Depositional model of the Rudník Lake during a lake-level highstand. Facies architecture was controlled mainly by subsidence along the northern marginal fault. The reconstruction incorporates postsedimentary northwestern dextral strike slip deformation of the basin. For explanation see text.

(Uronectes, Monicaris), and unidentified insects (Schneider and Zajíc, 1994; Zajíc, 1997). The diversified lake ecosystem including large predators such as 0.5–1 m long sharks needed sufficient time and water volume to develop.

4. Geochemical record

4.1. Approach

Several geochemical methods were applied in order to understand the response of the Rudník Lake to different climatic conditions reflected in changes of hydrological regime, water chemistry and bioproductivity. Stable isotopes of calcite have indicated the hydrological conditions in different basins (Talbot, 1990), boron content in clay is often closely associated with relative changes in palaeosalinity (Bohor and Gluskoter, 1973; Stewart and Parker, 1979; Goodarzi and Swaine, 1994), and organic geochemistry provides evidence about the biological source of organic matter, bioproductivity associated with nutrient supply and lake-level changes, redox conditions during transport and deposition, microbial degradation and diagenesis (Tissot and Welte, 1984).

4.2. Methods and samples

4.2.1. Stable isotopes of calcite

Most of the sampled rocks are well-laminated mudstones to limestones with low to very high organic matter content (up to 23% TOC) and with varying proportions of calcite and dolomite. Organic rich carbonate mudstones and carbonate laminites (facies Bs, La, Ml, Mc, Dm and Mo) were analysed to determine the stable isotopic composition of carbon and oxygen of calcite. Offshore facies in the Vrchlabí section and offshore as well as nearshore facies in the Kundratice section were sampled. A petrological study of thin sections allows five calcite phases to be recognised, which were analysed separately (Figs. 8, 9, 18): (1) Micrite of the black-grey, organic matter rich, clayey laminae of the carbonate mudstones (Bs, La and Mo facies). (2) Micrite to microspar of the grey clayey laminae of the carbonate mudstones with a lower organic matter content (Bs and Mo facies). (3) Whitish coarse pure microspar to fine-grained sparite lenticular laminae and lenses of assumed early diagenetic origin, containing very small admixtures of organic matter and clay minerals (Bs, La and Mo facies). (4) Microspar from laminae of carbonate mudstones with a dominant proportion of clay (Mc and Ml facies). (5) Microspar from nodular beds of muddy calcareous dolomite (Dm).

Types 1, 2 and 3 are referred to as primary, because they are believed to have been formed by the primary precipitation of micrite and microspar from lake water. No displacive/replacive structures were found in these samples.

Samples of laminated rocks, where different mineral phases occur in individual laminae, were taken using a dentist's microdrill. Calcium carbonate samples were decomposed under a vacuum in 100% H_3PO_4 at 25 °C (McCrea, 1950). Even though some samples contain a higher proportion of dolomite, more than 50% in a few samples, only calcium carbonate was decomposed at 25 °C, and higher temperatures for dolomite decomposition were not applied. All obtained values represent the samples' calcium carbonate phase. Released CO_2 was analysed on the Finnigan MAT 251 mass-spectrometer. The results are reported in per mil deviation from the V-PDB standard using the δ notation. The precision of both carbon and oxygen isotope analyses is better than ± 0.1‰. A total of 64 samples were analysed.

4.2.2. Organic petrology

Organic macerals were examined on polished surface samples of whole rocks using a UMSP 30 Petro microscope–photometer (Zeiss-Opton) at total magnification of 450× and 650×, under reflected non-polarized light and oil immersion ($n = 1.518$). Random reflectance was measured in monochromatic light of λ (wavelength) 546 nm. For fluorescence analyses a halogen discharge lamp and an F 109 filter set with blue light irradiation were used.

4.2.3. Elemental analysis, pyrolysis, gas chromatography and stable isotopes of organic matter

The total organic and total inorganic carbon contents (TOC and TIC, %) were measured using an ELTRA elemental analyser. Selected samples were analysed using a Rock-Eval 5 pyrolyser (Bordenave et al., 1993) in nitrogen flow with a temperature programme from 300 to 650 °C. A flame ionisation detector measured three parameters: 1) S1 — free (volatile) hydrocarbons (mg HC/g rock); 2) S2 — bound hydrocarbons and non-hydrocarbon compounds released by pyrolysis, S2 represents residual source potential (mg HC/g rock or kg HC/ tonne rock); 3) T_{max} — maximum temperature of the pyrolytic peak S2 (°C) that indicates the thermal maturity of kerogen.

The hydrogen index is calculated using the equation: HI = 100 * S2 / TOC (mg/g TOC) and represents the relative amount of hydrogen in kerogen molecules. This parameter is especially sensitive to organic facies.

Three samples were extracted by organic solvent (CH_2Cl_2) and the saturated hydrocarbon fraction analysed using capillary HP gas chromatography.

For mass-spectrometric analyses of the stable isotopic composition of organic carbon, carbonates were first removed by hot, diluted hydrochloric acid. The residue, after washing and drying, was combusted in a FISONS 1108 elemental analyser, which is coupled online with a Finnigan MAT 251 mass-spectrometer in continuous flow mode. The δ values were defined as the per mil deviation from the V-PDB standard. The reproducibility was ± 0.25‰.

A total of 13 samples of organic-rich rocks, mostly black shales and laminites of the Bs and La facies, were analysed. Samples with very high TOC content and samples with significant changes of $\delta^{18}O$ and $\delta^{13}C$ of calcite in vertical sections were selected for analysing the $\delta^{13}C$ of organic matter.

4.2.4. Distribution of boron in mudstones

A total of 65 samples of mudstones were crushed and then leached with 4% monochloracetic acid to remove carbonates from the suspension. The solid phase was decanted and washed by resuspension in distilled water. The clay fraction (< 2 μm) was decanted from non-settled matter in suspension. The mineralogy of the separated clay fraction of all samples was checked by the X-ray diffraction technique. The separated clay was digested with HNO_3 and HF in microwave dissociation equipment. The concentration of boron in the solution was determined by the ICP MS technique using Varian UltraMass equipment. Stable isotopic, Rock-Eval pyrolysis and gas chromatography analyses

Table 2
Random reflectance of organic macerals

Sample	R_r (%)	Sd	n	Description
Ca2/85.80	0.75	0.09	11	Vitrinite
V2/5	1.44	0.14	33	Inertinite (no vitrinite present)
V2/6	1.45	0.08	19	Inertinite (no vitrinite present)
V2/9	0.37	0.05	50	Liptinite (no vitrinite present)
K5	0.37	0.07	61	Liptinite (no vitrinite present)

R_r — random reflectance; Sd — standard deviation; n — number of measurements.

Table 3
Carbon and oxygen stable isotopes of calcite of carbonates

Sample	Metres in section	‰δ^{13}C (V-PDB)	‰ δ^{18}O (V-PDB)	Sample type
Vrchlabí section				
VB2	1.6	−3.4	−2.4	Matrix
VB3	2.3	−2.3	−3.3	Matrix
V2/3/A	2.35	−1.8	−2.6	Black matrix
V2/3/C	2.35	−0.6	0.4	Grey matrix
VB4/A	2.4	−0.8	0.2	Black matrix
VB4/B	2.4	−1.2	0.1	Grey matrix
VB4/C	2.4	−1.9	−0.7	Sparite
VB5	2.6	−1.7	−2.1	Matrix
VB6	2.65	−1.2	−3.5	Matrix
VB7/A	2.67	−0.9	−5	Black matrix
VB7/C	2.67	−0.1	−2.9	Sparite
VB8/A	2.7	−1.1	−4.6	Black matrix
VB8/C	2.7	−0.3	−3.1	Sparite
VB9/A	2.73	−1.4	−2.6	Black matrix
VB9/C	2.73	−1	−1.4	Sparite
VB 10	2.76	−3.1	−2.1	Matrix
VB11/A	2.8	−3.5	−4.1	Black matrix
VB11/C	2.8	−0.1	−1.7	Sparite
VB12	3	−3.1	−2.1	Matrix
V2/6/A	3.15	−0.3	−0.1	Black matrix
V2/6/b	3.15	−0.5	−0.1	Grey matrix
VB13	3.3	−2.2	−3.3	Matrix
VB 14/1	3.7	−3.1	−4.0	Grey matrix
VB 14/2	3.75	−2.5	−4.0	Grey matrix
VB 15/2	4.05	−2.8	−4.0	Matrix
VB 16/1	4.25	−2.4	−5.5	Grey matrix
VB 16/2	4.3	−1.3	−4.2	Grey matrix
VB 17	4.5	−2.0	−3.7	Grey matrix
VB 18	4.55	0.5	0.8	Matrix
VB 19/1	4.6	0.2	0.9	Black matrix
VB 19/2	4.6	−0.5	−2.0	Sparite
VB 20	4.65	0.6	−3.7	Matrix
VB 25	5.55	−2.7	−3.4	Grey matrix
VB 29	8.12	−5.1	−11.0	Grey matrix
Kundratice section				
KB 2	0.15	2.4	−4.8	Matrix
KB 4	0.32	1.7	0.2	Matrix
KB 5	0.38	2.5	1.3	Matrix
KB-6	0.45	2.1	0.1	Matrix
KB 7	0.50	−1.7	−2.4	Matrix
KB 8	0.55	−1.0	−3.1	Matrix
KB 9	0.60	−0.6	−2.7	Matrix
KB19	2.2	−2.2	−4	Matrix
KB20	2.6	−0.8	−5.7	Matrix
KB21/D	2.7	−1.1	−8.9	Clayey limy dolostone
KB22	2.76	1.7	−4.4	Matrix
KB 23	2.85	2.1	−5.9	Matrix
KB24	2.95	3.7	−3.2	Matrix
KB26	3.3	−1	−3.8	Matrix
Kundratice section				
K3F	3.6	−3.2	1.1	Clayey limy dolostone-centre
K3G	3.6	−4	−0.3	Clayey limy dolostone- margin
KB27	3.8	−1.1	−6.3	Matrix
KB50	4.1	−2.6	−5.7	Matrix
K4	4.3	−4	−0.6	Clayey limy dolostone-undifferentiated
KB 29	4.65	−1.1	−7.1	Mixed (both laminae)
KB29	4.65	−1.8	−7.2	Matrix
KB 35	6.55	1.0	−7.9	Mixed (both laminae)

were carried out by the laboratories of the Czech Geological Survey, boron determinations were done by the Geological Laboratories of Charles University.

4.3. Results

4.3.1. Stable isotopes of calcite

The values obtained are within the range of −11.0‰ to + 1.3‰ δ^{18}O and −5.1‰ to + 3.7‰ δ^{13}C (Table 3, Figs 12, 13). Calcite from shallow water muddy calcareous dolostones of the Dm facies shows higher δ^{18}O and lower δ^{13}C values in comparison to the rest of the data set (Fig. 12). The higher δ^{18}O and δ^{13}C values of pure microspar–sparite laminae, in comparison to the dark clayey organic-rich matrix laminae in most samples from the Vrchlabí section, can also be seen (Fig. 13). There is a covariant trend of grey matrix values with a high correlation coefficient $R=0.896$. Samples of primary calcite from Kundratice are richer in ^{13}C in comparison to the Vrchlabí section (Fig. 14).

In vertical sections, values of δ^{18}O and δ^{13}C show several distinctive features, the most striking of which is that δ^{18}O values follow the same trends as δ^{13}C values as noticed in many different lacustrine carbonates (e.g., Talbot, 1990; Talbot and Kelts, 1990), but this remains unsatisfactorily understood. At the base of the Kundratice section, a significant decrease in both δ^{18}O and δ^{13}C values can be seen at the transition from a black shale bed of Bs facies to the organic-rich carbonate bed of Co

Table 4
Total organic carbon (C_{TOC}), Rock-Eval pyrolysis parameters (S1, S2, Tmax) and calculated hydrogen index of organic-rich facies

Sample	Metres in section	Cmin (%)	C_{TOC} (%)	S1	S2	T_{max}	HI
Kundratice section							
KB1	0.07	7.21	12.19	1.9	44.66	433	366
KB2	0.15	7.09	11.47	2.38	41.86	433	365
KB3	0.25	5.81	14.49	3.33	48.72	434	336
KB4	0.32	7.06	10.36	3.79	40.42	433	390
KB5	0.38	7	12.11	4.37	46.16	434	381
KB6	0.45	4.23	10.42	4.58	40.18	430	386
KB7	0.5	8.44	1.99	1.54	10.48	430	527
KB8	0.55	8.55	1.1	1.07	5.8	424	527
KB9	0.6	8.96	0.99	0.91	5.16	426	521
KB20	2.6	1.7	2.15	0.31	5.38	430	250
KB21	2.7	0.7	17.35	2.59	48.84	426	281
KB22	2.76	4.22	19.59	3.88	60.16	434	307
KB23	2.85	5.04	17.74	4.24	58.34	437	329
KB24	2.95	3.92	13.47	4.88	48.16	434	358
KB25	3.1	0.65	23.13	5.44	61.02	427	264
KB26	3.3	4.88	0.87	0.21	1.88	428	216
KB29	4.65	1.24	1	0.06	0.88	435	88
KB34	6.4	MD	4.16	0.51	12.66	425	304
KB35	6.55	7.64	10.94	1.66	48.46	438	443
KB36	6.62	1.66	18.54	5.75	60.92	439	329
KB37	6.8	0.47	19.98	7.97	66.98	441	335
Vrchlabí section							
VB2	1.6	0.58	0.41	0.01	0.14	451	34
VB3	2.3	4.57	0.79	0.04	0.24	441	30
VB4	2.4	9	2.13	0.14	1.06	439	50
VB5	2.6	7	2.55	0.19	1.78	427	70
VB6	2.65	7.19	2.3	0.15	0.72	446	23
VB7	2.67	1.56	6.1	0.29	1.98	441	32
VB8	2.7	6.17	6.33	0.29	2.38	447	38
VB9	2.73	6.31	1.85	0.04	0.54	471	29
VB10	2.76	4.94	2.43	0.11	1.26	430	52
VB11	2.8	6.39	1.98	0.12	0.72	443	36
VB12	3	8.15	0.7	0.04	0.18	432	26
VB13	3.3	5.93	2.33	0.26	1.46	446	63
VB14.1	3.7	1.86	3.58	0.53	8.68	432	242
VB14.2	3.75	4.28	2.63	0.6	7.76	433	295
VB15.1	4	2.35	3.36	0.61	8.3	433	247
VB15.2	4.05	3.33	2.92	0.79	8.16	432	279
VB16.1	4.25	4.57	2.78	0.68	10.02	430	360
VB16.2	4.3	3.87	2.24	0.71	7.5	432	335
VB17	4.5	7.56	12.03	2.3	47.58	438	396
VB18	4.55	7.29	10.21	0.59	35.12	433	344
VB19	4.6	6.09	9.59	0.63	37.16	436	387
VB20	4.65	6.17	9.66	0.91	37.56	437	389
VB21	4.7	7.27	13.73	0.54	41.82	433	305
VB22	4.75	4.98	9.13	1.48	33.22	435	364
VB23	4.8	6.16	8.31	1.26	31.54	434	380
VB24	4.85	3.96	1.69	0.05	0.32	442	19
VB25	5.55	3.67	0.79	0.06	0.3	444	38
VB28	8.07	1.7	0.26	0.02	0.2	433	77
VB29	8.12	1.92	7.92	2.93	28.42	446	359

Abbreviation: MD, below detection limit.

facies (Fig. 15, 0.5 m, trend no. 2). Within the upper black shale bed (facies Bs, 2.7–3.3 m, trend no. 1) a gradual upwards increase in $\delta^{18}O$ and $\delta^{13}C$ values can be observed. Within the overlying near-shore facies both values decrease (3.3–4.8 m, trend no. 3). In the Vrchlabí section $\delta^{18}O$ and $\delta^{13}C$ values within the lower laminite bed (Fig. 16, La, 2.3–2.75 m, trend no. 1) show similar increasing upwards trends to $\delta^{18}O$ and $\delta^{13}C$ in the Kundratice upper black shale bed. Fluctuations in the $\delta^{18}O$ and $\delta^{13}C$ values are visible at the top of black shale (Bs) and at the bottom of the mudstone turbiditic unit (Mo, 2.7–3.3 m, trend no. 4).

4.3.2. Petrology and geochemistry of organic matter

The organic maceral composition was closely examined in eight samples of the anoxic facies Bs, La and the pelagic unit of Mo. The main petrographic features in most samples include a few micrometres to millimetres thick laminae, abundant occurrences of algal and amorphous organic matter commonly associated with terrestrial plant debris and framboidal pyrite (Figs. 17 and 18).

The major organic macerals identified following Taylor et al. (1998) comprise of: 1) Liptinite with benthic colonial algae, e.g., *Botryococcus braunnii*, or lamalginite (kerogen type I), sporinite and resinite (kerogen type II). 2) Amorphous organic matter formed by microbial decomposition of organic matter. 3) Dispersed mineral–bituminous groundmass (common) and exsudatinite filling fissures and voids (less common) visible in fluorescent light. 4) Fusinite and semifusinite with well-preserved cell walls and higher reflectance, which represents partly oxidized or charred terrestrial plant debris. 5) Vitrinite, the gelified humic substance (kerogen type III), which is present in many but not all samples as structureless collinite and telinite with partly visible plant tissues.

The proportions of the macerals vary in different lithologies and intervals. The maceral composition is closely associated with the geochemical parameters, e.g., hydrogen index or stable isotopes, and influences the apparent thermal maturity. Vitrinite reflectance (R_r) is commonly suppressed by 0.1–0.2% in samples rich in alginite. In many mudstone samples only fusinite, semifusinite and liptinites are identified (e.g., Table 2) and the thermal maturity was determined only from the T_{max} of the Rock-Eval pyrolysis. In both profiles the vitrinite reflectance varies from 0.6% to 0.8% and the T_{max} from 425 to 447 °C (Tables 2 and 4), corresponding to the beginning of the oil generative window (Bordenave et al., 1993; Tissot and Welte, 1984). The observed maceral composition and measured thermal maturity is in agreement with earlier studies of Permian rocks in this basin (Müller, 1987; Malán, 1989; Kříbek, 1990) aimed at oil shale prospecting and potential evaluation.

A total of 77 samples of organic-rich laminated mudstones, black shales and carbonates of facies Bs, La, Co and Mo from the Kundratice and Vrchlabí sections were analysed for total inorganic and organic carbon content (TIC and TOC, $\%_{wt}$) and 50 samples were analysed using Rock-Eval pyrolysis. The TOC values range from 0.10%$_{wt}$ to 13.73%$_{wt}$ in the Vrchlabí section and from 0.14%$_{wt}$ to 23.13% $_{wt}$ in the Kundratice section with an average value of 4.67% $_{wt}$ (Table 4, Figs. 15, 16, 19 and 20). The gas chromatograms of n- and isoprenoid alkanes of three characteristic samples in the Vrchlabí section are shown in Fig. 21.

The $\delta^{13}C$ values of total organic matter ($\delta^{13}C_{TOC}$) from the Vrchlabí and Kundratice sections are from −24.0‰ to −29.0‰ (Table 5), most of them are between −25‰ and −27‰. Covariance between carbon isotopic composition and organic matter content was not found. The differences in $\delta^{13}C_{calcite}$ and $\delta^{13}C_{TOC}$ are not homogeneous through the sections, but vary from 20.9‰ to 29.4‰.

Table 5
$\delta^{13}C$ of organic carbon in samples from Vrchlabí and Kundratice sections

Sample	Metres in section	$\delta^{13}C$ org. (‰ PDB)
Vrchlabí section		
V2/3/A	2.35	−26.9
VB4/A	2.4	−27.6
VB7/A	2.67	−25.4
VB8/A	2.7	−24.8
VB9/A	2.73	−25.3
VB11/A	2.8	−26
V2/6/A	3.15	−24.4
Kundratice section		
KB21/D	2.7	−26.30
KB22	2.76	−25.20
KB24	2.95	−25.70
KB26	3.3	−24.60
K3G	3.6	−26.6
K4	4.3	−25.70

4.3.3. Distribution of boron in mudstones

The average boron content in recent marine sediments is higher than in freshwater sediments (Goldschmidt and Peters, 1932; Reynolds, 1972). Water of some saline lakes can contain considerable amounts of boron; e.g., 360 ppm at Little Borax Lake in California (Livingstone, 1963). Because the boron content is almost unaffected by later diagenesis (Degens and Keith, 1959; Goldberg and Arrhenius, 1958) it has been used as a palaeosalinity indicator to discriminate ancient marine, brackish and freshwater sedimentary environments (e.g., Bohor and Gluskoter, 1973; Stewart and Parker, 1979; Goodarzi and Swaine, 1994). The boron content in mudstones can be covariant with Fe oxides/hydroxides due to preferential sorption to these minerals (Kraska, 1981b). In some Upper Cretaceous mudstone samples boron content covaries with organic matter content, reflecting preferential sorption of boron on organic matter (Uličný, 1989).

The boron content has already been used as a palaeosalinity indicator in the Upper Palaeozoic non-marine mudstones of the Bohemian Massif. Boron content has been interpreted as representing increasing aridity from the Late Carboniferous to the Late Permian (e.g., Bouška and Pešek, 1985, 1983, 1976). These authors did not consider the particular sedimentary environment of sampled mudstones, therefore the interpretation has a limited ability as evidence.

In this study we tested the hypothesis that boron can be used as a palaeoenvironmental indicator in the Upper Palaeozoic lacustrine deposits. The boron content in mudstones has been successfully used as a palaeosalinity indicator in different lacustrine strata of the Early Permian age in the same basin (Blecha et al., 1999).

Table 6
Boron contents in mudstones

Kundratice section			Vrchlabí section			Čistá 2 borehole		
Sample	Boron ppm	Metres in section	Sample	Boron ppm	Metres in section	Sample	Boron ppm	Metres in section
KB 47	343	−5.00	VB 1	250	1.1	Ča-2	348.7	35.7
KB 46	359	−4.40	VB 2	179	1.6	Ča-2	280.2	37.8
KB 45	381	−3.75	VB 3	236	2.3	Ča-2	328	43.3
KB 43	355	−1.60	VB 5	147	2.6	Ča-2	345.4	46.8
KB 40	432	−0.10	VB 6	142	2.65	Ča-2	436.5	51.2
KB 1	98.1	0.10	VB 7	73	2.75	Ča-2	337.1	53.3
KB 3	241	0.25	VB 12	434	3	Ča-2	331.6	56.2
KB 12	566	0.88	VB 13	535	3.3	Ča-2	283.8	57.9
KB 16	403	1.20	VB 14/1	425	3.7	Ča-2	212	61.5
KB 17	417	1.40	VB 14/2	337	3.75	Ča-2	233.4	64.3
KB 18	496	1.80	VB 16/1	388	4.25	Ča-2	204.5	68.2
KB 19	377	2.20	VB 16/2	359	4.3	Ča-2	268.1	71.4
KB 20	359	2.60	VB 17	278	4.5	Ča-2	306.7	78.6
KB 22	169	2.76	VB 21	246	4.75	Ča-2	230.6	82.4
KB 25	152	3.10	VB 24	373	4.95	Ča-2	212.9	84.5
KB 26A	389	3.30	VB 25	423	5.55	Ča-2	293	85.8
KB 26B	428	3.30				Ča-2	193.9	86.95
KB 27	603	3.80				Ča-2	318.1	103.8
KB 50	376	4.10				Ča-2	265.9	105.9
KB 28	542	4.35				Ča-2	301.7	106.6
KB 29	407	4.65				Ča-2	212.8	108.6
KB 51	339	4.70				Ča-2	182.3	110.5
KB 32	334	5.50						
KB 33	294	6.00						
KB 35	95	6.55						
KB 36	81.6	6.65						
KB 37	117.5	6.80						

4.3.3.1. Results. Values of boron in the separated clay fraction (< 2 μm) are in the range from 73 to 603 ppm, the average value being 350 ppm. In the Kundratice section values are from 82 to 603 ppm (Table 6, Fig. 15), in the Vrchlabí section (Table 6, Fig. 16) from 73 to 535 ppm and in the Čistá 2 borehole (Table 6, Fig. 5) from 194 to 437 ppm.

The main mineral components detected by X-ray diffraction are quartz, analcite, 10 Å fraction (illite, hydrated muscovite), 7 Å fraction (chlorite, kaolinite), feldspars (orthoclase as well as plagioclases) and a small amount of hematite.

The covariance between boron content and mineral composition was investigated by statistical methods. Spearman's rank correlation coefficient was calculated for each mineral phase (Johnová, 1996). No correlation between boron values and analcite was found ($r=0.088$); there was a very low correlation between boron and illite and/or muscovite ($r=0.262$), quartz ($r=0.355$), kaolinite and/or chlorite ($r=0.564$) and hematite ($r=-0.326$). The portion of samples that could covary is less than 10% for all calculated relationships.

The covariance between boron and organic matter (OM) content was also tested. Boron analyses were carried out in the same 30 samples as before and after removal of OM by heating to 450 °C, respectively. The values of boron content after removing OM are slightly higher, which approximately correspond to a loss of the samples' total weight (samples with higher TOC content show a proportionally higher shift in boron values, Johnová, 1996).

4.4. Interpretation of geochemical results

4.4.1. Stable isotopes of calcite

Longinelli (1996 and references therein) emphasized experimental work, which proved that carbon–

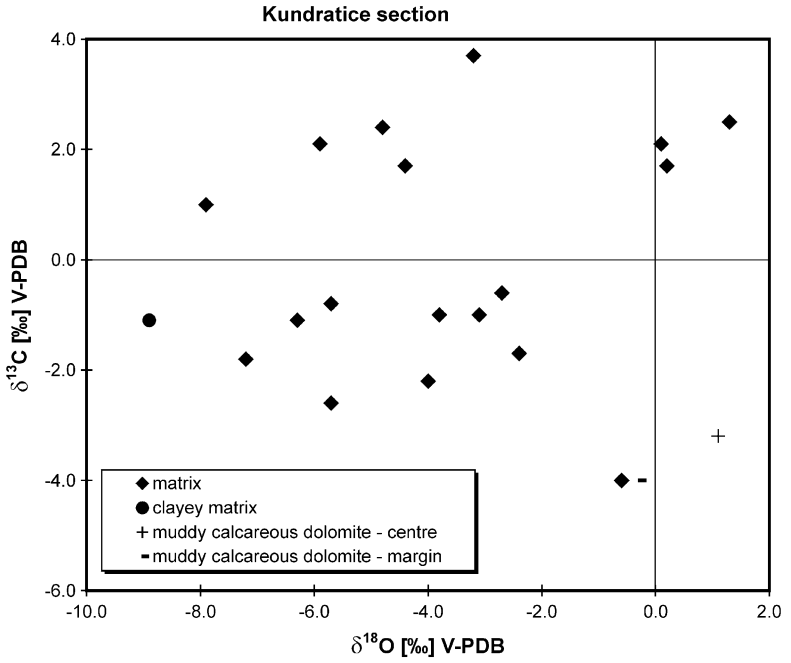

Fig. 12. The $\delta^{18}O/\delta^{13}C$ plot of calcite from samples of the Kundratice section.

oxygen bonds in carbonates are not stable and the isotopic composition can be substantially modified during diagenesis. We believe that our data reflect the primary and early diagenetic composition of calcite. The first reason is the lack of displacive and/or replacive structures and the preservation of primary and early diagenetic structures. Additionally diagenetic overprint would probably cause homogenisation of values, but our data show substantial changes of δ values in vertical sections, within individual beds, even between individual adjoining laminae. Finally a diagenetic overprint may cause a shift of all samples in sections towards more rich or depleted values. Therefore our interpretations are based mainly on vertical sections' relative changes of values.

The $\delta^{18}O$ and $\delta^{13}C$ values from both sections fall in the range of freshwater limestones (Hoefs, 1997). Samples of primary calcite from Kundratice are richer in ^{13}C in comparison to the Vrchlabí section (Fig. 14), which can be ascribed to higher bioproductivity in a more restricted environment.

Higher $\delta^{18}O$ and lower $\delta^{13}C$ values of calcite from shallow water muddy calcareous dolostones of the Dm facies (Fig. 12) can be interpreted in terms of enrichment by ^{12}C from partly decaying organic matter, which is present in the surrounding mudstones as well as the dolostone itself. The higher $\delta^{13}C$ values of pure microspar–sparite laminae, in comparison to the dark clayey organic-rich matrix laminae in most samples from the Vrchlabí section, can be explained by hypertrophic conditions during summer (Fig. 13). Kelts and Hsü (1978) described seasonal lacustrine lamination with pure microspar summer laminae precipitated during algal blooms. Shifts of calcite stable isotopic values from the calculated equilibrium reflects eutrophication; hypertrophic conditions led to precipitation of much larger calcite crystals — up to 50 μm (Teranes et al., 1999). Most of the pure microspar–fine spar laminae of the Rudník Lake anoxic offshore deposits show these features, therefore we interpret them as a seasonally bioinduced precipitation. Enrichment in ^{18}O can be caused by higher evaporation/salinity during hypertrophic conditions.

Fig. 13 also shows a covariant trend of the grey matrix values with a high correlation coefficient $R=0.896$. Primary calcite precipitated from hydrologically closed lakes show covariance of ^{13}C and ^{18}O values (Talbot, 1990), and lakes with $R=0.7$ and higher are considered as hydrologically closed. We suppose, that the Rudník Lake was hydrologically

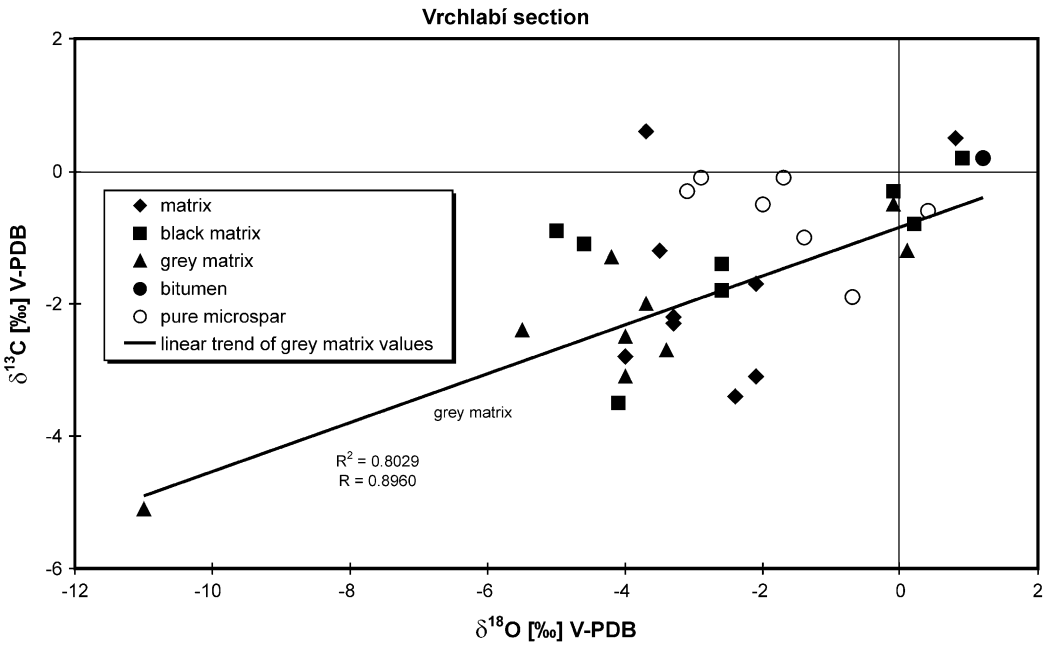

Fig. 13. The $\delta^{18}O/\delta^{13}C$ plot of calcite from samples of the Vrchlabí section. The covariant trend of clay matrix values is discussed in the text.

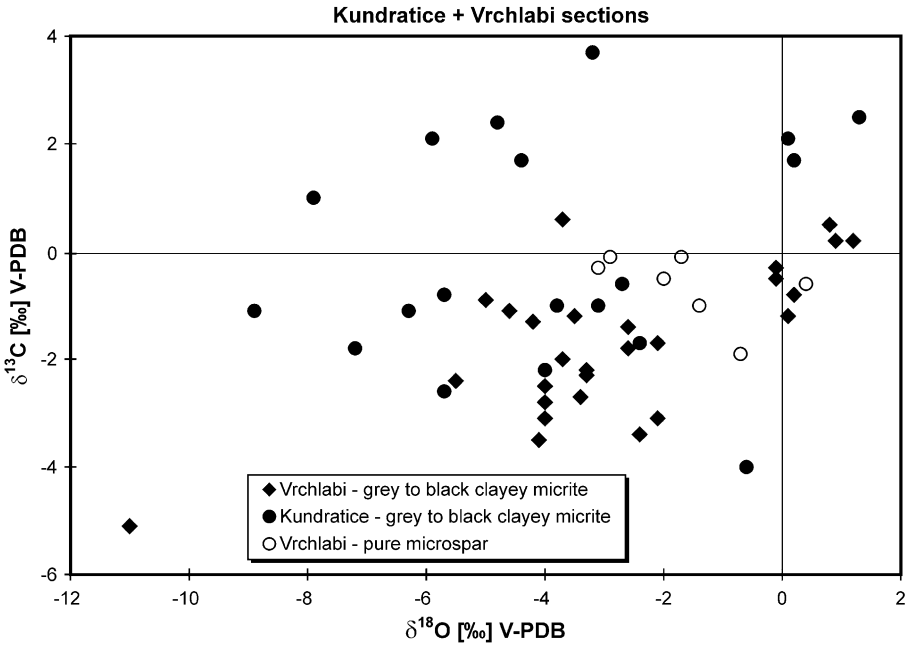

Fig. 14. Summary $\delta^{18}O/\delta^{13}C$ plot of calcite from samples of the Vrchlabí and Kundratice sections showing higher $\delta^{13}C$ of samples from Kundratice.

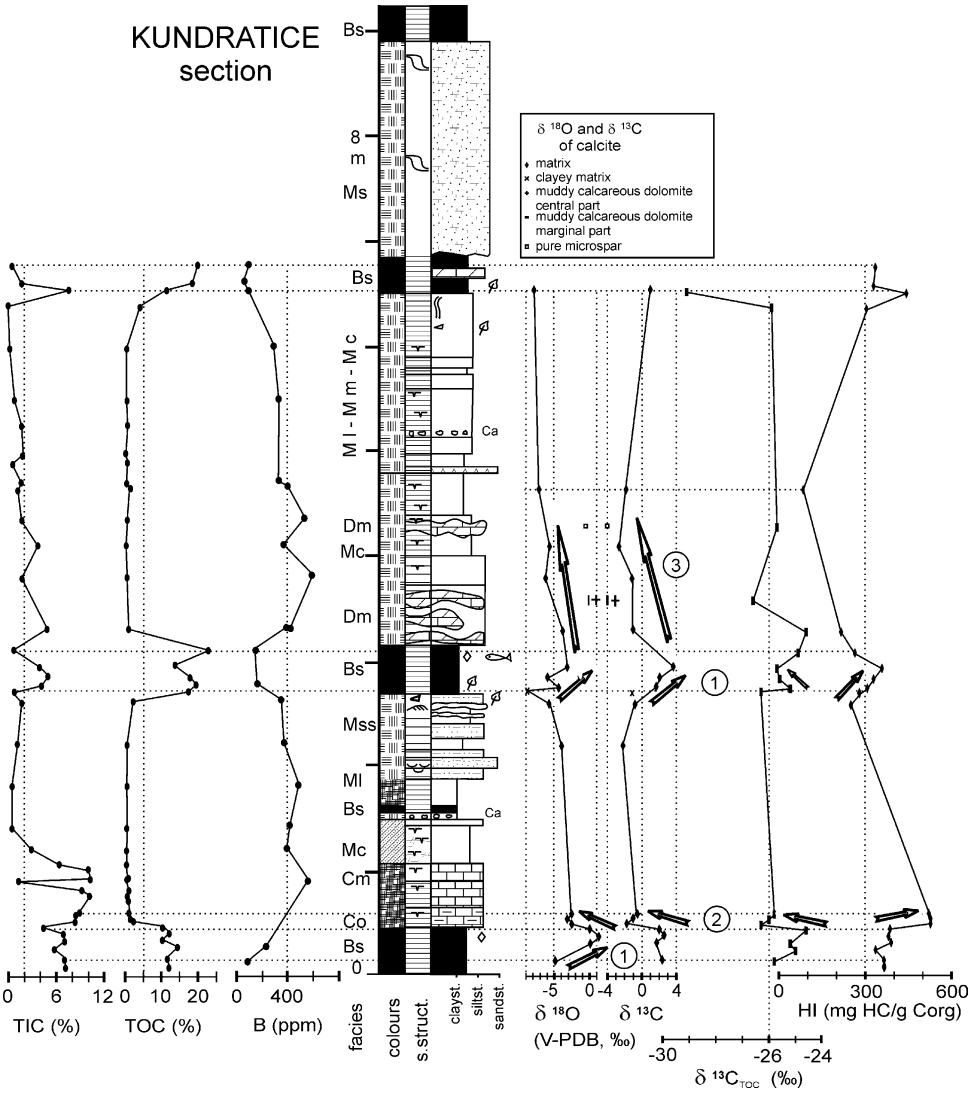

Fig. 15. Log of the Kundratice section showing distribution of total organic carbon (C_{TOC}), total carbonate carbon (Cmin), boron, $\delta^{18}O$ and $\delta^{13}C$ of calcite, $\delta^{13}C$ of organic matter, and hydrogen index. Circled numbers refer to different vertical trends discussed in the text.

closed at least during the precipitation of grey matrix samples (Vrchlabí section, Fig. 16). Samples of grey, clay-rich matrix are scattered along the section from the bottom to the top (2.4–8.12 m), and are mostly from rocks with no distinctive fine lamination or from rocks, where three types of laminae, black, grey and whitish, were present.

4.4.2. Hydrogen index (HI)

The TOC data are plotted against S2 (bound hydrocarbons) and cluster into four major groups (Fig. 20). The slopes of the trend lines are proportional to the hydrogen indexes (HI) and are characteristic for specific kerogen types (Talbot et al., 2004). The first group of rocks with a very high TOC of 8–23%$_{wt}$ and S2 30–60 mg/g comprises black shales and laminites from the later stage of lake development and eutrophication. These are excellent source rocks with very good hydrocarbon generative potential. The second group consists of mudstones and calcareous dolomite with a similar kerogen type as the first group (both have an HI of 322 mg/g TOC) but are more diluted by the mineral matrix

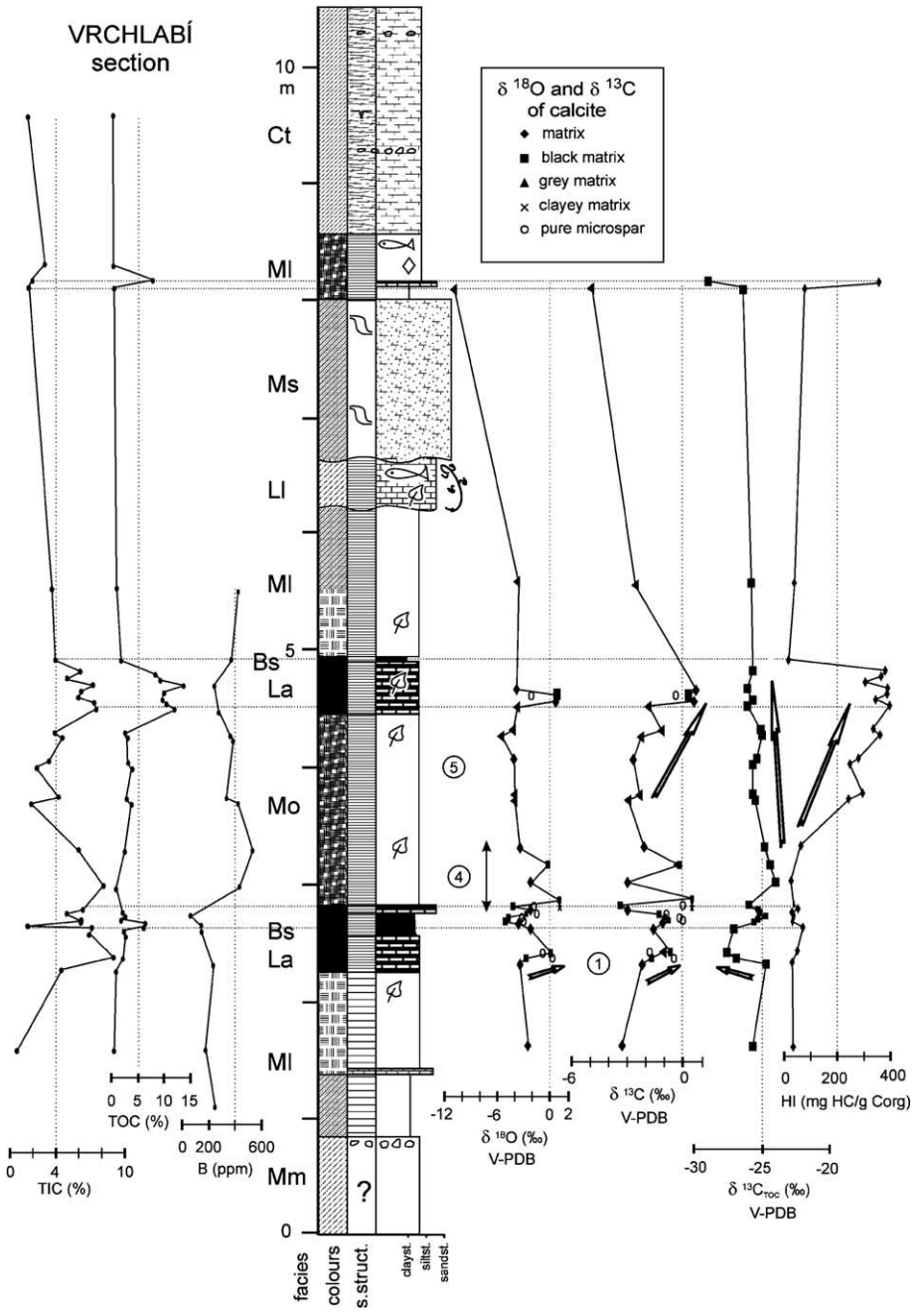

Fig. 16. Log of the Vrchlabí section showing distribution of total organic carbon (C_{TOC}), total carbonate carbon (Cmin), boron, $\delta^{18}O$ and $\delta^{13}C$ of calcite, $\delta^{13}C$ of organic matter, and hydrogen index. Circled numbers refer to different vertical trends discussed in the text.

and hence have a lower organic matter concentration. The organic rich carbonates have a relatively low TOC, 1–2%, but the quality of kerogen is very high (average HI = 552 mg/g TOC) due to the high amount of algae and scarcity of fusinite or other terrestrial plant debris. The last group, with the lowest hydrogen index (HI = 33 mg/g TOC), comprises of laminites and black shales from the initial stage of lake development. The kerogen

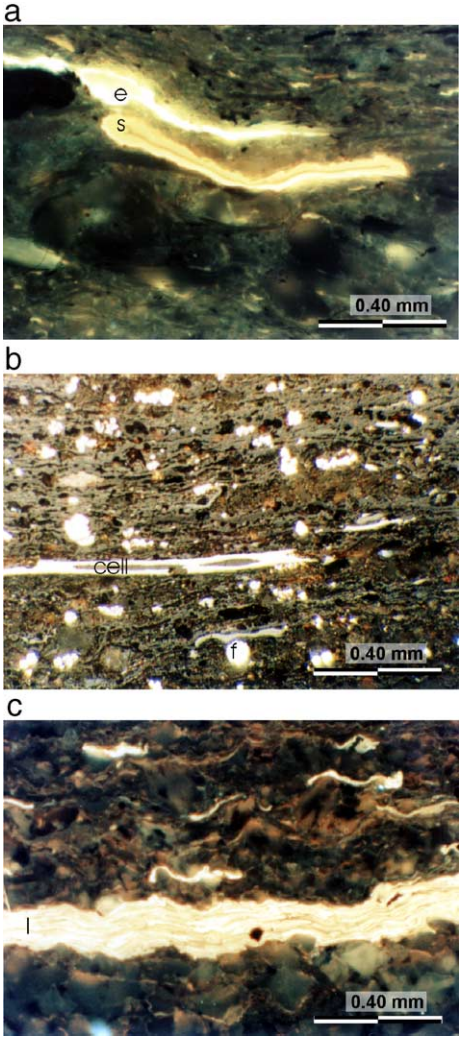

Fig. 17. a) Black shale (Bs facies). Matrix (grey) rich in carbonate with a small amount of dispersed liptodetrinite; high intensity hydrocarbon (e — exsudatinite) originated from deformed spore (s) in the centre (lower intensity). Čistá 2 section, 85.80 m, polished section, UV light. b) Black shale (Bs facies). Detail of lamina rich in organic matter. Large fusinite particle showing some faint cell structure (in the centre, high intensity reflectance). Highest intensity framboidal (circular) particles of pyrite are abundant (f). Matrix is formed by amorphous organic matter with clay minerals (upper part of section, light grey). Lamalginite forms dark elongated grains. Kundratice section, 0.2 m, polished section, reflected light. c) Kundratice 0.2 m in UV light. Lamalginite (high intensity) forms dispersed elongated particles and discrete lamina (in the centre) (l). Matrix is rich in carbonate grains with exsudatinite coatings. Compare also to Fig. 8. b).

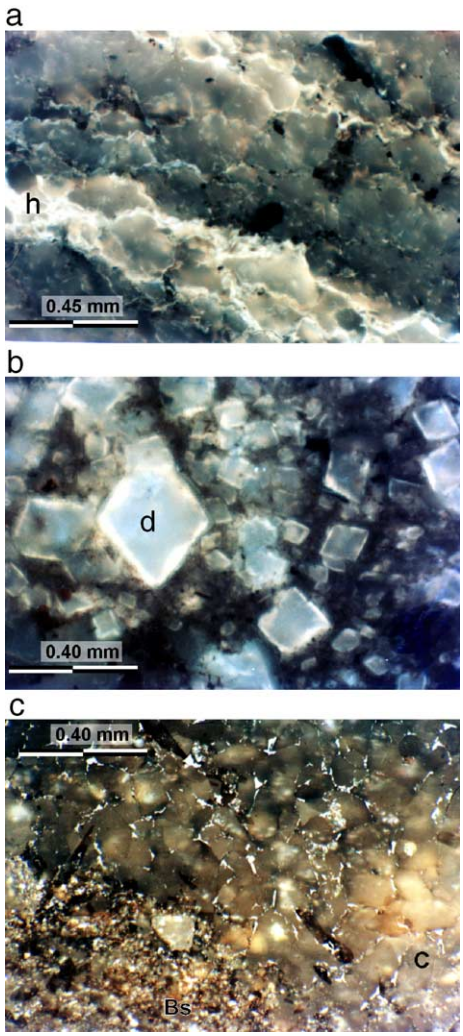

Fig. 18. a) Organic-rich dolomite bed enclosed in black shales (facies Bs). Hydrocarbon (exsudatinite, bright) coatings on carbonate grains. Laminae rich in hydrocarbons (high intensity) (h) alternate with laminae of pure carbonate (dark). Kundratice section, 6.7 m, polished section, UV light. b) Organic-rich mudstone (facies Mo). Detail of silty carbonate lamina showing zoned dolomite rhombs (d) in clay matrix. Vrchlabí section, 3.2 m, polished section, UV light. c) Vrchlabí section, 3.2 m in reflected light. White heterogeneous migrabitumen coatings in detrital carbonate grains (larger grey crystals). Sharp contact between fine-grained black shale laminae (Bs), lower left and silty carbonate lamina (C), upper right is also seen. Polished section, reflected light.

is rich in fusinite, semifusinite and other humic substances derived from land plants. Only minor differences are observed between the two sections. The Vrchlabí section does not reach as high a concentration

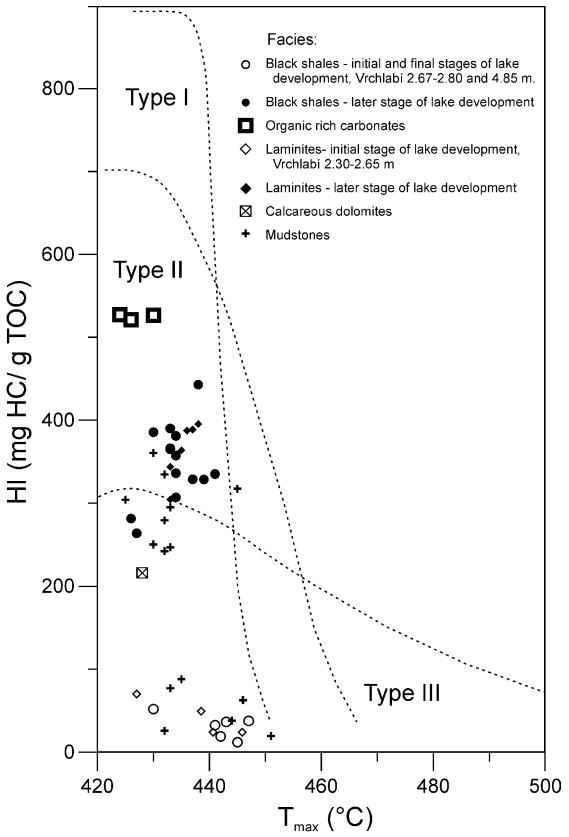

Fig. 19. Plot of hydrogen index (HI) versus Tmax values with main types of kerogen. Most of the samples are mixtures of algal and terrestrial organic matter (type II) formed during the later stages of lake development, but some samples are enriched in kerogen type III and are dominated by terrestrial plant debris transported to the lake during its initial stage of development.

and quality of organic matter as the rocks in the Kundratice section, probably due to its position in a deeper part of the basin closer to the northern, steeper slopes of the rising Krkonoše Mountains, which provided higher detrital influx into the basin.

The plot of the hydrogen index in relation to thermal maturity expressed by T_{max} show the envelopes of major kerogen types and their thermal degradation during diagenesis (Fig. 19). At the time of deposition, the original HI values were probably higher and the organic-rich carbonates would have plotted as typical type I kerogen. Yet, the thermal diagenetic overprint is not very high and the organic matter parameters still indicate many aspects of the evolving palaeo-environment.

Several trends are apparent in vertical sections (Figs. 15 and 16). In the Vrchlabí section between 1.6 and 4.8 m a striking upward increasing trend of HI values is shown (Fig. 16). In the Kundratice section a similar trend can be seen within the upper black shale bed (2.7–3.1 m) and a large shift of HI to higher values at the transition from the basal black shale bed to the organic-rich carbonate (0.5 m). These trends are interpreted as a record of algal blooms and lake eutrophication.

4.4.3. Saturated hydrocarbons in rock extracts

The distribution of the saturated hydrocarbons with n-alkanes (n-C10 .. n-C38) and isoprenoid hydrocarbons (ip-C13 .. ip-C20) in the rock extracts shows several organic matter characteristics and a depositional environment in three selected lithologies and lake development stages (Fig. 21). The black shale (Fig. 21, Vrchlabí section VB 2.7 m, Bs) has a distinct predominance of n-alkanes over the isoprenoids, pristane/phytane (ip-C19/ip-C20) ratio close to 1.1 and odd/even predominance in the n-C13 to n-C18 range. These characteristics are typical of dysoxic conditions in the water column and predominantly plankton-derived organic matter (Tissot and Welte, 1984). The organic matter rich mudstone (Fig. 21, Vrchlabí section VB 4.5 m, Mo) is strikingly different with pristane/phytane < 1 typical for reducing conditions in the water column. Abundant higher alkanes with notable odd/even predominance in the n-C25 .. n-C33 range and isoprenoids > n-alkanes in the lower molecular range suggest early thermal maturity and significant contribution of terrestrial plant debris to the kerogen composition. High hopane content (next to n-C31) indicates possible microbial reworking of the deposited organic matter. The laminite sample (Fig. 21, Vrchlabí section VB 4.6 m, La) shows maximum abundant n-alkanes around n-C15 .. n-C17 with odd/even predominance in this range and a high n-alkanes/isoprenoids ratio, a pristane/phytane ratio close to 1 and low amounts of n-alkanes in the n-C25–32 range. This pattern is characteristic for dysoxic carbonate depositional environments with high algae and low terrestrial input.

4.4.4. Stable isotopes of organic carbon

The $\delta^{13}C$ values of biological material are determined by the isotopic composition of the carbon source and by isotopic fractionation of carbon during photosynthesis and metabolic reactions. Diagenetic

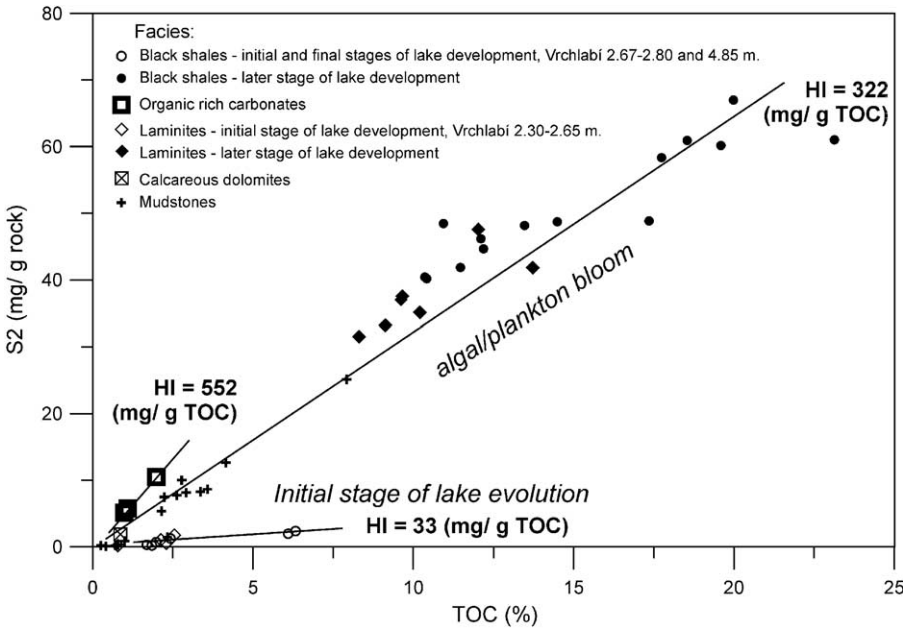

Fig. 20. Characterisation of organic matter by pyrolytic hydrocarbons (S2) and total organic carbon (TOC). The slope of the trendlines is proportional to the Hydrogen Index (HI). Symbols depict different lithologies and form clusters related to palaeoenvironmental settings. The highest HI is observed in organic-rich carbonates with almost pure indigenous planktonic algae kerogen, the lowest HI occurs in sediments with redeposited terrestrial plant detritus rich in inertinite.

alteration commonly leads to a small shift towards a ^{13}C depletion of 1–2‰ (Galimov, 1980). This shift is common to all kerogens that have experienced similar diagenetic alteration. The high range in $\delta^{13}C$ values (at least several ‰) of sedimentary organic matter should reflect primary isotope heterogeneities in the biological precursor material (Arneth, 1984).

Hemicellulose, proteins and pectins are enriched in ^{12}C relative to bicarbonate by about 17‰, cellulose and lignin by 23‰ and lipids by 30‰ (Degens et al., 1968). It follows that organic material rich in lipids, such as algae, shows lower $\delta^{13}C$ values than organic matter formed from terrestrial plants rich in lignin, such as coal. The respective average $\delta^{13}C$ values of Carboniferous coals from the Polish Silesian Basin are about −23.5‰, the Saar coals −24.4‰ and the Aachen coals −23.9‰ $\delta^{13}C$ (Rice and Kotarba, 1993). Modern plants with C3 metabolism have $\delta^{13}C$ values from −23.1‰ to−27.9‰ (Meyers, 1990). It is possible to assume that samples from the Rudník member contained organic matter rich in lignin and cellulose (kerogen type III, with low HI) with $\delta^{13}C$ values close to −24‰, organic matter rich in lipids with lower $\delta^{13}C$ values and high HI, and a mixture of both types.

The differences in $\delta^{13}C$ values of calcite and organic matter, which were calculated for all samples, vary from 20.9‰ to 29.4‰. The wide range of $\Delta\delta^{13}C$ values could be explained by different carbon sources for calcite and organic matter; diagenetic alteration of calcite is probably of minor importance. Organic matter redeposited from the coast and rivers was brought into the lake as sedimentary organic matter, which was not necessarily oxidised and calcite precipitated from lake water with a different $\delta^{13}C$ composition of total dissolved carbon (TDC). Carbonate and organic matter was not necessarily formed in the same water column depth. Concentrations and carbon isotopic compositions of CO_2 in lakes from New England (USA) show CO_2 $\delta^{13}C$ values of about −8.6‰ for water from shallow water layers (epilimnion), whereas $\delta^{13}C$ values of CO_2 from deeper in the water column are from −10‰ to −22.6‰ (Oana and Deevey, 1960). Lower $\delta^{13}C$ values in deeper water are explained by the higher portion of CO_2 originating from organic matter decomposition.

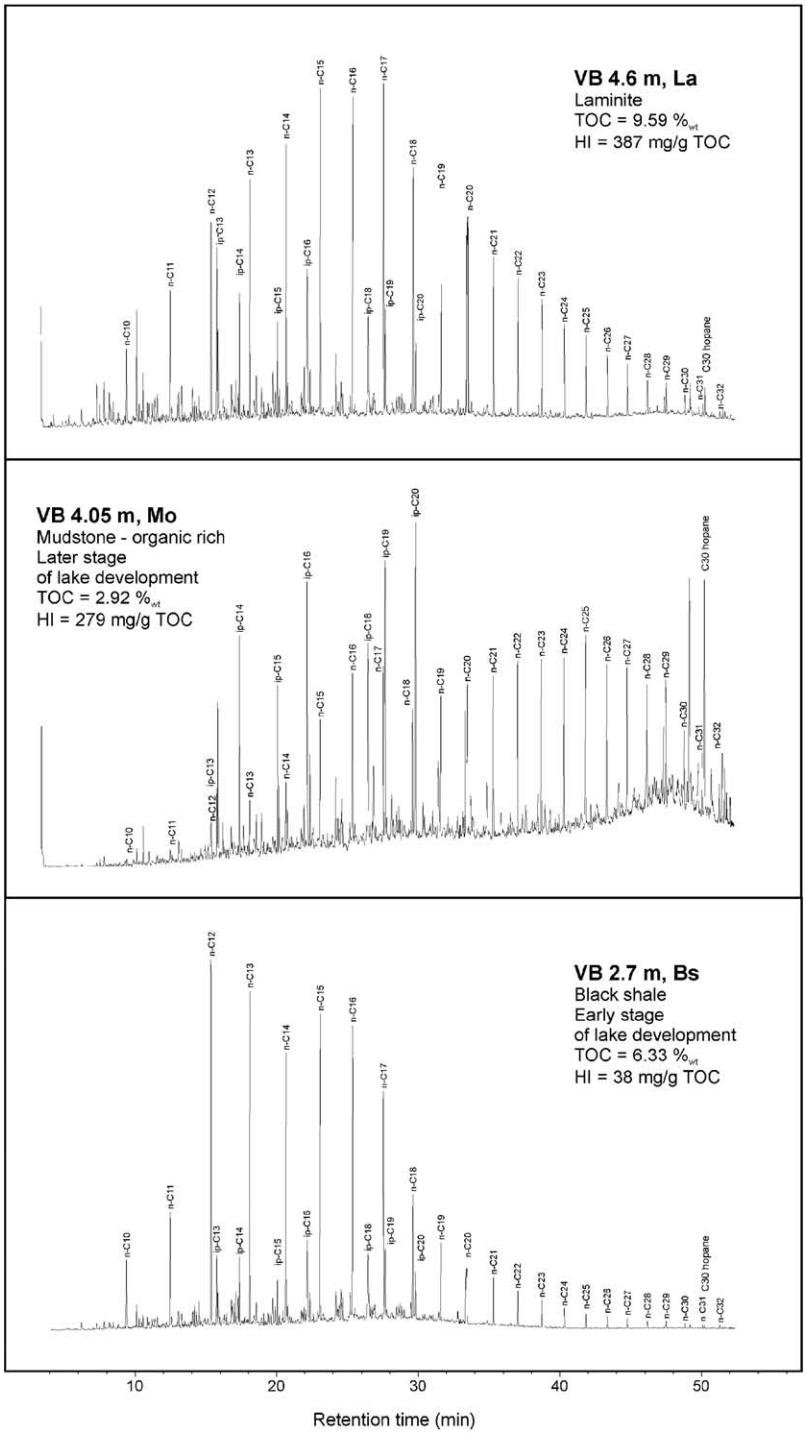

Fig. 21. Distribution of the saturated hydrocarbons in rock extracts of three characteristic lithologies and lake evolution stages in the Vrchlabí section.

4.4.5. Vertical trends of geochemical parameters

The onset of low $\delta^{18}O$ values at the base of several black shale and laminite beds and gradually increasing upwards trend of $\delta^{18}O$ values in the upper parts of these beds probably records the onset of the highest lake level (trend no. 1, Fig. 15, Vrchlabí section 2.3–2.5 m, Fig. 16, Kundratice section 0.1–0.4 and 2.7–3.0 m). The maximum proportion of meteoric water was during a humid period and the importance of evaporation increased gradually during a later, more arid, period (see Talbot, 1990). A consequent gradual drop in lake level can be supposed. In some places (Kundratice 2.7–3.1 m, Vrchlabí 2.2–2.6 m) oxygen isotopic trends are accompanied by upwards increasing $\delta^{13}C_{calcite}$ and HI values and decreasing $\delta^{13}C_{TOC}$, indicating increasing bioproductivity in the lake, which can be interpreted in terms of a shift towards a warmer climate. The abundance of mostly juvenile fish fossils at 3.0 m in Kundratice can most easily be explained by eutrophication (Zajíc, 1997), which fits very well with the geochemical data. The highest TOC values (23%) suggest intensified anoxic conditions during this stage of basin evolution.

The large shift of HI to higher values, the highest in the dataset, in the Kundratice section at the transition from the basal black shale bed to the organic-rich carbonate (Fig. 16, 0.5 m, trend no. 2) can be explained by a reflection of transgressive or highstand conditions with low siliciclastic and low degraded OM input and high primary productivity. Also rapid carbonate precipitation, which enables better preservation of aquatic OM can explain high HI values. Large shifts of $\delta^{18}O$ and $\delta^{13}C_{calcite}$ values in this part of the section can be interpreted as a result of different sources of calcium carbonate during precipitation of carbonate bed. This can be caused by changes in source area or bloom of plankton or necton with calcareous tests (e.g., Ostracods reported by Zajíc, 1997); the increase in bioproductivity is indicated by a shift of $\delta^{13}C_{TOC}$ towards more negative values.

The gradual upwards decreasing trends of $\delta^{18}O$ and $\delta^{13}C_{calcite}$ values in the Kundratice section within the muddy nearshore succession (Fig. 16, 3.3–4.8 m, trend no. 3) can be ascribed to lake water gradually mixing with, for example, river water rich in pedogenic ^{12}C.

Several types of offshore facies occur in the Vrchlabí section. The transition from basal laminites to the muddy turbidites (Fig. 15, 2.9–3.3 m, trend no. 4) is characterized by a high variation in $\delta^{18}O$ and $\delta^{13}C$ values which can be interpreted as a record of the different proportions of primary and redeposited material in particular samples. It could also be a record of lake level fluctuations in a hydrologically closed regime and significant changes in the isotopic composition of TDC in lake water caused by changes in bioproductivity and different proportions of pedogenic CO_2 transported from the land. A general upwards increasing trend in $\delta^{13}C_{TOC}$ values in this part of the section can be explained in terms of an increasing portion of land-derived organic matter and a decrease in phytoplankton organic matter during the onset of turbidite sedimentation.

The upper part of the Vrchlabí section (Fig. 15, 3.3–4.8 m, trend no. 5) has generally low and homogeneous $\delta^{18}O$ values accompanied by upward increasing trends in $\delta^{13}C_{calcite}$ and HI values and upwards decreasing $\delta^{13}C_{TOC}$ trend. Stable and low oxygen isotope values can be ascribed to lake-level highstand and hydrologically open conditions during most of this period (cf. Talbot, 1990). The significant upward trend of increasing HI and $\delta^{13}C_{calcite}$ and decreasing $\delta^{13}C_{TOC}$ provide evidence of increasing bioproductivity during this time (Talbot and Livingstone, 1989; Neumann et al., 2002).

The Kundratice section is characterized by higher HI and higher total organic matter contents compared to the Vrchlabí section. It is interpreted as reflecting a generally higher bioproductivity and lower input of redeposited terrestrial material due to the position of the Vrchlabí section close to the palaeo-shoreline of the steep northern basin margin.

4.4.6. Boron

Mudstone mineralogy, the presence of volcanogenic or organic material, and mineralogy within the source area are the main factors assumed to influence the palaeosalinity record (e.g., Curtis, 1964; Spears, 1965; Kraska, 1981a). Covariance between boron content and mineral composition or TOC content were not found. The studied sections represent a relatively short period of time and so we do not interpret any substantial changes in sediment provenance. Finally volcanogenic material was found in only one bed (facies Ms) in the Vrchlabí and Kundratice sections. These observations led us to interpret changes in boron content of mudstones of the Rudník Lake deposits as reflecting changes in palaeosalinity.

In the Kundratice section, the offshore facies show the lowest boron values (from 82 to 241 ppm), which are interpreted as a record of low lake water salinity during lake-level highstands. The nearshore mudstones and siltstones of facies Mss, Mo and Ml show higher values (294–496 ppm), and mudflat facies Mc exhibit the highest values (542–603 ppm). This is interpreted as a record of higher lake water salinity during lower lake levels. In the Vrchlabí section the lowest values are also concentrated in the anoxic offshore facies (Bs and La, 73–246 ppm) representing highest lake level. The highest values occur in the muddy turbidites (Mo, 337–535 ppm). An increase of values in the lower part of Mo succession is probably related to a large fall in lake level and muddy turbidite sedimentation could have been triggered by such lake level fluctuations. In the Čistá 2 section anoxic offshore facies (Bs) show the lowest values (205–268 ppm) as well. The highest values (293–437 ppm) were recorded within mud-cracked mudstones of mudflat (Mc) facies. Absolute values of boron content in different sections are not compared, because they probably represent more or less different lacustrine subsystems of different palaeo-hydrochemistry history and different clay mineralogy.

Higher salinity during the lake-level lowstand indicates hydrologically closed conditions; on the contrary, lower salinity during the lake highstand, which was stable for a relatively long time, can indicate hydrological opening of the lake during highstand. The distribution of boron in the studied sections indicates substantial changes in lake water salinity, which was related to lake level changes recorded by sedimentary facies. Lake level was driven mainly by a precipitation/evaporation ratio, so lake level changes must have been induced by climatic changes.

5. Summary and discussion

Highstand periods of the Rudník Lake are recorded in most sections by the deposition of organic-rich finely laminated mudstones and carbonates. High organic content (up to 10–23% of TOC), common presence of autochthonous organic matter, abundant pyrite and lack of bioturbation indicate high bioproductivity and anoxic bottom conditions. The lake must have been eutrophic to oligotrophic with well-developed stratification for most of the year. Two types of seasonal lamination within the anoxic organic-rich offshore facies are present. The first consist of clayey organic-rich dark laminae alternating with whitish pure microspar laminae in La facies (cf. Kelts and Hsü, 1978). The pure microspar laminae are considered to represent late summer bioinduced calcite precipitation during algal blooms. The second type of lamination, found in several Bs facies beds, comprises almost pure algal laminae alternating with clay-dominated laminae (Fig. 8a, b). These probably also reflect seasonal algal blooms but under different conditions. The lack of carbonate within these deposits can be explained by low carbonate input and the resulting low carbonate content in lake water or by acid conditions in the hypolimnion, which prevent accumulation of carbonate minerals due to their dissolution near the lake bottom. Low carbonate input seems improbable, because these black shales are usually overlain by carbonates. Dissolution of carbonates in the hypolimnion can be due to the high concentrations of CO_2 released from decaying OM (Dean and Fouch, 1983; Pilskaln, 2004). Eutrophic lake deposits may thus contain less carbonates in comparison to the lower productivity lake deposits situated in a similar source area and climatic setting (Dean, 1981). High aridity, high temperature and a rainfall regime in the seasonal Pangean interior during the Early Permian are the principal common conclusions of most climatic models (Barron and Fawcett, 1995). Therefore the Bohemian Massif could have been in the zone of influence of seasonal monsoons occurring in the peri-Tethys region.

The widespread presence of dolomite in most carbonate and mudstone facies of the Rudník Lake deposits is interpreted as mostly the product of primary precipitation, because of a lack of displacive structures. Primary precipitation of dolomite in lacustrine settings is widely accepted (Hardie, 1987; Tucker and Wright, 1990), but requires waters highly supersaturated with carbonate ions and a high Mg/Ca ratio, which are restricted to evaporitic conditions. Most of the non-detrital dolomite found in recent and Quaternary lakes come from saline lakes (Last, 1990). We propose a model of primary precipitation of high Mg calcite and protodolomite for the Rudník Lake deposits, which could soon have been early diagenetically modified to dolomite, a process which does not require extensive neomorphism. Degradation of organic matter could

raise pH, ionic strength and carbonate alkalinity, which are, in addition to Mg supply, substantial factors controlling dolomite precipitation (Slaughter and Hill, 1991). The source of Mg could have been intrabasinal basic volcanic rocks and low-grade Lower Palaeozoic metasediments surrounding the basin, which contain abundant chlorite and basic metavolcanics.

The study of vertical changes in boron content in the clay fraction of the lacustrine mudstones shows that high lake level stages were periods of lower salinity, and periods of falling lake level were followed by significant increases in salinity. This could reflect climatic variability with humid periods reflected by a relatively hydrologically more open state (recorded by low boron values of offshore deposits) and more arid periods by a hydrologically closed state (indicated by increase of boron values in nearshore/mudflat deposits).

A vertical trends of upward increasing $\delta^{18}O$, $\delta^{13}C_{calcite}$ and HI and decreasing $\delta^{13}C_{TOC}$ (Figs. 15 and 16) are interpreted as reflecting an increase in bioproductivity and lake-level lowering. They probably represent change from a relatively humid to a warmer and more arid climate. An increase in $\delta^{18}O$ could reflect an increase in the evaporation/precipitation ratio, which can be most likely explained in terms of lake level lowering during the onset of a more arid and warmer period.

Another vertical trend characterized by the increase of $\delta^{13}C_{calcite}$ and HI, and by a decrease of $\delta^{13}C_{TOC}$ followed by stable and relatively low $\delta^{18}O$ values (Figs. 15 and 16) probably reflects an increase in bioproductivity during the periods of high lake level and probably hydrologically open regime, indicated by low and stable oxygen values. An increase of hydrogen index and TOC can indicate a rise of lake level, due to the better OM preservation of an oxygen-depleted lake bottom during high lake level stages (Talbot and Livingstone, 1989). The low and stable $\delta^{18}O$ values in calcite of the Rudník Lake deposits, however, do not reflect any substantial change in the $^{18}O/^{16}O$ ratio in the lake water, which would have followed rise in lake level. The increase in bioproductivity during the stable high lake level can be caused by higher nutrient supply and/or a change of climate to warmer and more humid conditions. The highest lake-level was controlled by topography, discharge, and could not have been further increased by more humid conditions.

The basin was in a hydrologically closed state during the low lake levels. Millimetre–centimetre thick intercalations of early diagenetic displacive gypsum, found in the red mudstone-dominated succession overlying the Rudník Lake deposits, indicate continuing hydrologically closed basin conditions and the high water output/input ratio in the Rudník Lake.

During the Permian most of the Pangean interior was arid, and a positive water budget is proposed only in some peri-Tethys areas influenced by monsoons (Barron and Fawcett, 1995). Average July temperatures of the area where the Bohemian Massif was situated during the Early Permian, were around 20–25 °C and January average temperatures between 25–30 °C (Crowley et al., 1989). According to these climatic models the Pangean interior was characterised by high climate continentality and seasonality with large differences between day/night and summer/winter temperatures. Which corresponds to our interpretation of the carbonate/black shale laminites of the Rudník Lake deposits as products of seasonal lamination (see chapter 3). The Bohemian Massif was situated between 2° and 4° N Early Permian latitude (Krs and Pruner, 1995), and a hot semiarid climate is expected, which can most easily explain the well-established stratification, periods of high bioproductivity, and high rate of evaporation leading to substantial drops of lake level and increasing salinity, $^{18}O/^{16}O$ ratio and carbonate ion concentrations in the lake water.

Several orders of climatic cyclicity are recorded in the Rudník Lake deposits. Lake-level fluctuations recorded by transgressive/regressive facies units several metres to tens of metres thick, probably represent periods of tens to possibly hundreds of kyr (section Čistá 2, Fig. 5). Higher salinity during lowstands and lower salinity during highstands can most easily be explained by more arid and humid climatic conditions, respectively. Lake-level and bioproductivity fluctuations in the order of kyr or possibly hundreds of years, recorded by stable isotopes and OM geochemistry, are very probably climatically driven. The seasonal lamination represents the highest-frequency climatic record of the Rudník Lake.

Quaternary analogues can help the understanding of such climatic oscillations. Tropical African lakes were subject to a major dry period and low lake-levels during the last glacial maximum (~18 kyr BP) (Talbot and Johannessen, 1992; Gasse et al., 1989; Johnson et

al., 2000; Stager et al., 2002; Trauth et al., 2001), which are ascribed to a weakening of the Afro-Asian monsoon (Stager et al., 2002). A similar pattern was found by Benson et al. (1998) in mid-latitude Mono Lake (California). In Lake Tanganyika the water-level fluctuations are in phase with glacioeustatic sea-level changes (Gasse et al., 1989).

The two main maxima of the Late Palaeozoic glaciation are suggested as being in the Westphalian and Sakmarian; based on the extent of ice-rafted deposits (Frakes et al., 1992). The Asselian, when the Rudník Lake was formed, was a period when the Sakmarian glacial period initiate. Lake level changes of the Rudník Lake may reflect climatic oscillations of the order of tens of thousands years, comparable to lower orders of glacial/interglacial cycles. Evidence of glacial/interglacial climatic oscillations in the equatorial environments has only been rarely documented. Milankovitch-type climatic cyclicity was found by Olsen and Kent (1996) in lacustrine cycles of the Upper Triassic Newark Supergroup and by Fredriksen et al. (1998) in lacustrine/aeolian/fluvial cycles of the Permian Brodrick Beds, Scotland. Triassic playa deposits in Germany with a cyclicity driven by a Pangean monsoon-like system were changing intensity within the Milankovitch frequency band (Reinhardt and Ricken, 2000).

6. Conclusions

1. Four facies associations recognized within the Rudník Lake deposits are interpreted as: a) anoxic offshore deposits (pelagic, finely laminated black shales, carbonate/black shale laminites and carbonates), b) suboxic to oxic offshore deposits (pelagic to hemipelagic laminated grey, variegated to red mudstones and carbonates), c) nearshore and mudflat deposits (nearshore sandstones, sandstone/mudstone heterolithics, carbonates, mudflat mudstones), and d) gravity driven deposits (turbidite sandstones, distal turbidite silty mudstones, debrite conglomerates).
2. The lateral distribution of sedimentary facies with high gradient facies (turbidites, debris flows) and the thickest offshore facies succession distributed along the present-day northern basin margin, and much thinner offshore facies successions and low-gradient facies (mudstone and carbonate dominated), found in the south and south-west of the basin, point to the asymmetry of Rudník Lake deposits.
3. The apparent asymmetry of the basin fill and the distribution of sedimentary facies reveal an original half-graben basin geometry. Subsidence along the northern basin margin fault was the main factor controlling large-scale facies architecture of the Vrchlabí Formation (Asselian) within the basin. A substantial increase in subsidence rate was probably responsible for the formation of the large (300–500 km^2), relatively deep and long-lived lacustrine system of the Rudník Lake.
4. The observed seasonal lamination is in agreement with climate models for the Early Permian.
5. The Rudník Lake was a complex lacustrine system with well-developed offshore and nearshore zones, a stratified water column, periods of high and mainly algal bioproductivity and eutrophication which favoured the accumulation of large amounts of hydrogen-rich kerogen in the sediments: TOC is up to 23% and HI > 500 mg/g.
6. Major lake level fluctuations of the Rudník lacustrine system, recorded by shallowing-up facies units in most sections throughout the basin, were followed by significant changes in lake water salinity, reflected by changes in boron content in the clay fraction of mudstones. The highstands were periods of hydrologically more open conditions and lower salinity, indicated by the low boron values. The lowstands, on the other hand, were characterized by higher salinity and higher boron values. This is interpreted as a response to an increase in the evaporation/precipitation ratio in a hydrologically closed lake.
7. Lake level fluctuations of the Rudník Lake can also be traced in the monotonous offshore facies-dominated section, where no sedimentological evidence of lake-level changes exists. Evidence of such changes is documented by variations in $\delta^{18}O$ and $\delta^{13}C$ values of primary calcite, $\delta^{13}C$ and Hydrogen Index (HI) of organic matter. In the first case, an upward-increase of $\delta^{18}O$, $\delta^{13}C_{calcite}$ and HI and a decrease of $\delta^{13}C_{TOC}$ in vertical sections are interpreted as a result of increased

bioproductivity and lake-level lowering. It probably represents a change in climate from relatively humid to a warmer and more arid period. In the second case, the increase in $\delta^{13}C_{calcite}$ and HI, and decrease in $\delta^{13}C_{TOC}$ followed by stable and relatively low $\delta^{18}O$ values reflect an increase in bioproductivity during a period of high lake level and probably a hydrologically more open regime. This can be interpreted as the transition to warmer conditions during a stable, humid climate period.

Acknowledgements

The research was performed with the support of the Grant Agency of the Czech Republic project No. 205/94/0692, Ministry of Education project No. MSM 113100006 and by kind permission of the Aquatest Co. We wish to thank V. Prouza and R. Tásler for their suggestions, discussions and help with selecting suitable outcrops and to Harry Shaw and Karel Žák for discussions and thorough reviews of the first versions of the manuscript. We gratefully acknowledge the anonymous editor and three reviewers for improving the manuscript and for additional references. K.M. also wish to thank to J. Zajíc, Z. Šimůnek and J. Drábková for help with understanding palaeoecological and biostratigraphical aspects. Many thanks to Richard Withers for English review. Most of the work was done by K. Martínek as part of his PhD thesis.

Appendix A. The geographic coordinates of the localities and wells studied

Outcrop/well	*X* (WGS84)	*Y* (WGS84)	*Z* (metres)
Honkův Potok	15°23′20″ E	50°37′10″ N	415
HPK-1	15°21′54.46″ E	50°35′41.93″ N	332.87
Kv-1	15°24′10.62″ E	50°34′23.91″ N	352.53
Kundratice	15°25′40″ E	50°34′35″ N	385
Lt-1	15°25′11.88″ E	50°33′26.37″ N	368.04
Ba-2	15°26′1.83″ E	50°31′52.37″ N	438.24
Ro-1	15°25′24.58″ E	50°31′5.57″ N	411.03
Vrchlabí	15°35′50″ E	50°37′25″ N	510
Prostřední Lánov	15°39′35″ E	50°37′35″ N	380
Ča-2	15°41′26.49″ E	50°37′1.06″ N	506.75
HK-1	15°36′4.30″ E	50°34′6.05″ N	435.00
HPK-9	15°25′55.06″ E	50°32′26.47″ N	371.81

References

Alexander, J., Leeder, M.R., 1987. Active tectonic control on alluvial architecture. In: Ethridge, F.G., Flores, R.M., Harvey, M.D. (Eds.), Recent Developments in Fluvial Sedimentology, Spec. Publ. SEPM, vol. 39, pp. 143–252.

Allen, P.A., Allen, J.R., 1990. Subsidence history. In: Allen, P.A., Allen, J.R. (Eds.), Basin Analysis, Principles and Applications. Blackwell Science, pp. 263–281.

Arneth, J.D., 1984. Stable isotope and organo-geochemical studies on Phanerozoic sediments of the Williston basin, North America. Isot. Geosci. 2, 113–140.

Barron, E.J., Fawcett, P.J., 1995. The climate of Pangea: a review of climate model simulations of the Permian. In: Scholle, P.A, Peryt, T.M., Ulmer-Scholle, D.S. (Eds.), The Permian of Northern Pangea, vol. 1. Springer-Verlag, pp. 37–52.

Benson, L.V., Lund, S.P., Burdett, J.W., Kashgarian, M., Rose, T.P., Smoot, J.P., Schwartz, M., 1998. Correlation of Late-Pleistocene lake-level oscillations in Mono Lake, California, with North Atlantic climate events. Quat. Res. 49, 1–10.

Blair, T.C., Bilodeau, W.L., 1988. Development of tectonic cyclothems in rift, pull-apart, and foreland basins: sedimentary response to episodic tectonism. Geology 16, 517–520.

Blecha, M., Martínek, K., Drábková, J., Šimůnek, Z., Zajíc, J., 1997. Environmental changes at the Carboniferous/Permian Boundary and their Impact on the Floral and Faunal Assemblages of the Fossiliferous Lacustrine Horizons of the Krkonoše Piedmont Basin. Final Report, Project GAČR 205/94/0692, Czech Geological Survey, Prague, Czech Republic (in Czech).

Blecha, M., Martínek, K., Mihaljevič, M., 1999. Sedimentary and geochemical record of the ancient Kalná Lake, Lower Permian, Krkonoše Piedmont Basin, Czech Republic. Acta Univ. Carol. 43 (4), 657–665.

Bohor, B.F., Gluskoter, H.J., 1973. Boron in illite as an indicator of paleosalinity of Illinois coals. J. Sediment. Petrol. 43, 945–956.

Bordenave, M.L., Espitalie, J., Leplat, J., Oudin, J.L., Vandenbroucke, M., 1993. Screening techniques for source rock evaluation. In: Bordenave, M.L. (Ed.), Applied Petroleum Geochemistry. Editions Technip, Paris, pp. 217–278.

Bouška, V., Pešek, J., 1976. The geochemical role of boron in the Carboniferous sediments of Czechoslovakia. Proceedings of the 7th Conference on Clay Mineralogy and Petrology, Karlovy Vary, pp. 203–209.

Bouška, V., Pešek, J., 1983. Boron in the Permo–Carboniferous aleuropelites of the Bohemian Massif, Czechoslovakia. Proceedings of the 9th Conference on Clay Mineralogy and Petrology, Zvolen, 1982, pp. 209–216.

Bouška, V., Pešek, J., 1985. Boron in the aleuropelites of the Bohemian Massif. 5th Meeting of the European Clay Groups, Prague, 1983. Charles University, Prague, pp. 147–155.

Bush, M.B., Miller, M.C., De Oliveira, P.E., Colinvaux, P.A., 2002. Orbital forcing signal in sediments of two Amazonian lakes. J. Paleolimnol. 27, 341–352.

Coward, M.P., 1986. Heterogeneous stretching, simple shear and basin development. Earth Planet. Sci. Lett. 80, 325–336.

Crowell, J.C., Link, M.H. (Eds.), 1982. Geologic History of the Ridge Basin, Southern California. — Los Angeles, Pacific Section. Society of Economic Paleontologists and Mineralogists, pp. 1–304.

Crowley, T.J., Hyde, W.T., Short, D.A., 1989. Seasonal cycle variations on the supercontinent of Pangea: implications for Early Permian vertebrate extinctions. Geology 17, 457–460.

Csato, I., Kendall, C.G.S.C., Nairn, A.E.M., Baum, G.R., 1997. Sequence stratigraphic interpretations in the southern Dead Sea basin, Israel. GSA Bull. 108, 1485–1501.

Curtis, C.D., 1964. Studies on the use of boron as a paleoenvironmental indicator. Geochim. Cosmochim. Acta 28, 1125–1137.

Dam, G., Surlyk, F., 1993. Cyclic sedimentation in a large wave- and storm-dominated anoxic lake; Kap Stewart Formation (Rhaetian–Sinemurian), Jameson Land, East Greenland. In: Posamentier, H.W., Summerhayes, C.P., Haq, B.U., Allen, G.P. (Eds.), Sequence Stratigraphy and Facies Associations, IAS Spec. Publ, vol. 18, pp. 419–448.

Dean, W.E., 1981. Carbonate minerals and organic matter in sediments of modern north temperate hardwater lakes. In: Ethridge, F.G., Flores, R.M. (Eds.), Recent and Ancient Non-marine Environments: Models for Exploration, Spec. Publ. SEPM, vol. 31. SEPM, Tulsa, pp. 213–231.

Dean, W.E., Fouch, T.D., 1983. Lacustrine environment. In: Scholle, P.A., Bebout, D.G., Moore, C.H. (Eds.), Carbonate Depositional Environments, AAPG Memoir, vol. 33. AAPG, Tulsa, pp. 97–130.

Degens, E.T., Keith, M.F., 1959. Geochemical indicators of marine and freshwater sediments. Res. Geochim., pp. 38–61.

Degens, E.T., Behrendt, M., Gotthardt, G., Reppmann, E., 1968. Metabolic fractionation of carbon isotopes in marine plankton. II. Data on samples collected off the coasts of Peru and Ecuador. Deep-Sea Res. 15 (1), 11–20.

Drábková, J, 1997. Palynology of Rudník horizon. In: Blecha, M., Martínek, K., Drábková, J., Šimůnek, Z., Zajíc, J. (Eds.), Environmental Changes at the Carboniferous/Permian boundary and their Impact on the Floral and Faunal Assemblages of the Fossiliferous Lacustrine Horizons of the Krkonoše Piedmont Basin. (in Czech). Final Report, Project GAČR 205/94/0692, Czech Geological Survey, Prague, Czech Republic, pp. 104–111 (in Czech).

Drábková, J., Šimùnek, Z., Zajíc, J., 1990. Paleontologické zpracování sbìrù z lokality Vrchlabí- záøez silnice na jz. okraji mìsta. Report. Czech Geological Survey, Praha, pp. 1–83 (in Czech).

Frakes, L.A., Francis, J.E., Syktus, J.I., 1992. Climate Modes of the Phanerozoic. Cambridge University Press, UK.

Fredriksen, K.S., Clemmensen, L.B., Lawætz, H.S., 1998. Sequential architecture and cyclicity in Permian desert deposits, Brodrick Beds, Arran, Scotland. J. Geol. Soc. (Lond.) 155, 677–683.

Freyet, P., Plaziat, J.C., 1982. Continental carbonate sedimentation and pedogenesis, Late Cretaceous and Tertiary of Southern France. Contribution to Sedimentology, vol. 12. Schweizerbartsche Verlagsbuchhandlung, Stuttgart, pp. 1–273.

Galimov, E.M., 1980. $^{13}C/^{12}C$ in kerogen. In: Durand, B. (Ed.), Kerogen, Ch. 9. Technip, Paris, pp. 271–291.

Gasse, F., Ledee, V., Massaul, M., Fontes, J.C., 1989. Water-level fluctuations of lake Tanganyika in phase with oceanic changes during the last glaciation and deglaciation. Nature 342, 57–59.

Gastaldo, R.A., DiMichele, W.A., Pfefferkorn, H.W., 1996. Out of the icehouse into the greenhouse: a Late Paleozoic analog for modern global vegetational change. GSA Today 6, 1–7.

Gawthorpe, R.L., Leeder, M.R., 2000. Tectono-sedimentary evolution of active extensional basins. Basin Res. 12, 195–218.

Gawthorpe, R.L., Fraser, A.J., Collier, R.E.L., 1994. Sequence stratigraphy in active extensional basins: implications for the interpretation of ancient basin-fills. Mar. Pet. Geol. 11, 642–658.

Goldberg, E.D., Arrhenius, G.O.S., 1958. Chemistry of Pacific pelagic sediments. Geochim. Cosmochim. Acta 13, 153–212.

Goldschmidt, V.M., Peters, C., 1932. The geochemistry of boron: I, II.— Nachr. Ges. Wiss. Gottingen, Math.–Physik. K1., 402–407, 528–545.

Goodarzi, F., Swaine, D.J., 1994. Paleoenviromental implications of the boron content of coals. Bull. - Geol. Surv. Can. 471, 1–76.

Hardie, L.A., 1987. Dolomitization a critical view of some current views. J. Sediment. Petrol. 57, 166–183.

Hoefs, J., 1997. Stable Isotope Geochemistry, 4th ed. Springer-Verlag, Berlin.

Huc, A.Y., Le Fournier, J., Vandenbroucke, M., Bessereau, G., 1990. Northern Lake Tanganyika — an example of organic sedimentation in an anoxic rift lake. In: Katz, B.J (Ed.), Lacustrine Basin Exploration — Case Studies and Modern Analogs, AAPG Memoir, vol. 50. AAPG, Tulsa, pp. 169–185.

Janaway, T.M., Parnell, J., 1989. Carbonate production within the Orcadian basin, northen Scotland — a petrographic and geochemical study. Palaeogr. Palaeoclimatol. Palaeoecol. 70, 89–105.

Johnová, R., 1996. Boron as an paleosalinity indicator in the Czech Permo–Carboniferous. Bc. thesis, Charles University, Prague. (in Czech).

Johnson, T.C., Halfman, J.D., Showers, W.J., 1991. Paleoclimate of the past 4000 years at lake Turkana, Kenya, based on the isotopic composition of authigenic calcite. Palaeogr. Palaeoclimatol. Palaeoecol. 85, 189–198.

Johnson, T.C., Kelts, K., Odada, E., 2000. The Holocene history of Lake Victoria. AMBIO 29, 2–11.

Kelts, K., Hsü, K.J., 1978. Freshwater carbonate sedimentation. In: Lerman, A. (Ed.), Lakes, Chemistry, Geology, Physics. Springer Verlag, New York, pp. 295–323.

Kraska, F., 1981a. Die Bormethode. Wiss. Z. Ernest-Moritz-Arndt-Univ. Greifsw. 30, 9–18.

Kraska, F., 1981b. Kritische Bemerkungen zur Bormethode. Wiss. Z. Ernest-Moritz-Arndt-Univ. 30, 19–26.

Kříbek,B., 1990. Uhlíkaté formace a jejich úloha při metalogenezi Českého masívu. DrSc thesis, Karlova Universita, Praha. (in Czech).

Krs, M., Pruner, P., 1995. Paleomagnetism and paleogeography of the Variscan formations of the Bohemian Massif, comparison with other European regions. J. Czech Geol. Soc. 40/1–2, 3–46.

Last, W.M., 1990. Lacustrine dolomite— an overview of modern, Holocene, and Pleistocene occurrences. Earth Sci. Rev. 27, 221–263.

Liro, L.M., 1993. Sequence stratigraphy of a lacustrine system: Upper Fort Union Formation (Paleocene), Wind River Basin, Wyoming, U.S.A. AAPG Mem. 58, 317–333.

Livingstone, D.A., 1963. Chemical composition of rivers and lakes. U.S. Geol. Surv. Prof. Pap. 440-G.

Longinelli, A., 1996. Pre-Quaternary isotope palaeoclimatological and palaeoenvironmental studies: science or artifact. Chem. Geol. 129, 163–166.

Malán, O., 1989. Organic petrology. In: Hošek (Ed.), Bituminous Shales in Krkonoše Piedmont Area. Final Report. MS Geofond, Geoindustrie, Praha. (in Czech).

Martinsen, O.J., Ryseth, A., Helland-Hansen, W., Flesche, H., Torkildsen, G., Idil, S., 1999. Stratigraphic base level and fluvial architecture: Ericson Sandstone (Campanian), Rock Springs Uplift, SW Wyoming, USA. Sedimentology 46 (2), 235–259.

McCrea, J.M., 1950. The isotopic composition of carbonate and paleotemperature scale. J.Chem. Phys. 18, 849–857.

Meyers, P.A., 1990. Impacts of Late Quaternary fluctuations in water level on the accumulation of sedimentary organic matter in Walker Lake, Nevada. Palaeogeogr. Palaeoclimatol. Palaeoecol. 78, 229–240.

Müller, P., 1987. Pyrolýza Rock-Eval a stanovení C_{TOC}, Cmin v horninách podkrkonošského permokarbonu a cyprisového souvrství (in Czech). Report, Czech Geological Survey, Brno.

Muir, M., Lock, D., von der Borch, C., 1980. The Coorong model for Penecontemporaneous Dolomite Formation in the Middle Proterozoic McArthur Group, Northern Territory, Australia. Spec. Publ. SEPM 28, 51–67.

Neumann, T., Stogbauer, A., Walpersdorf, E., Stuben, D., Kunzendorf, H., 2002. Stable isotopes in recent sediments of Lake Arendsee, NE Germany: response to eutrophication and remediation measures. Palaegeogr. Palaeclimatol. Palaeoecol. 178, 75–90.

Oana, S., Deevey, E.S., 1960. Carbon-13 in lake waters and its possible bearing on paleoclimatology. Am. J. Sci. 258A, 253–272.

Olsen, P.E., 1986. A 40-million-year lake record of Early Mesozoic orbital climatic forcing. Science 234 (4778), 842–848.

Olsen, P.E., Kent, D.V., 1996. Milankovitch climate forcing in the tropics of Pangaea during the Late Triassic. Palaegeogr. Palaeclimatol. Palaeoecol. 122, 1–26.

Pilskaln, C.H., 2004. Seasonal and interannual particle export in an African Rift Valley lake: a 5-year record from Lake Malawi, southern East Africa. Limnol. Oceanogr. 49, 964–977.

Platt, N.H., Wright, V.P., 1992. Palustrine carbonates and the Florida Everglades; towards an exposure index for the fresh-water environment. J. Sediment. Petrol. 62, 1058–1071.

Posamentier, H.W., Allen, G.P., 1999. Siliciclastic sequence stratigraphy: concepts and applications. SEPM Concepts in Sedimentology and paleontology, vol. 7.

Prouza, V., Tásler, R., 2001. Krkonoše Piedmont Basin. In: Pešek, J. (Ed.), Geologie a ložiska svrchnopaleozoických limnických pánví České republiky. Czech Geological Survey, Praha, pp. 128–166 (in Czech).

Prouza, V., Šimùnek, Z., Zajíc, J., 1997. A new locality of the Rudník Horizon (Autunian) in the Mnichovo Hradiště Basin at Proseè pod Ještìdem (in Czech). Czech Geological Survey Reports in 1996. Czech Geological Survey, Praha, pp. 37–38.

Reinhardt, L., Ricken, W., 2000. The stratigraphic and geochemical record of Playa Cycles: monitoring a Pangaean monsoon-like system (Triassic, Middle Keuper, S. Germany). Palaegeogr. Palaeclimatol. Palaeoecol. 161, 205–227.

Reynolds, R.C., 1972. Boron: element and geochemistry. In: Fairbridge, R.W. (Ed.), The Encyclopedia of Geochemistry and Environmental Sciences. Van Nostrand Reyhold Co., New York, pp. 88–90.

Rice, D.D., Kotarba, M., 1993. Origin of Upper Carboniferous coalbed gases, Lower and Upper Silesian coal beds, Poland. Proceedings of the 1993 International Coalbed Methane Symposium, pp. 649–658.

Ricketts, R.D., Johnson, T.C., 1996. Climate change in the Turkana basin as deduced from a 4000 year long delta O-18 record. Earth Planet. Sci. Lett. 142, 7–17.

Rider, M.H., 1996. The Geological Interpretation of Well Logs. Blackie, Glasgow, United Kingdom.

Rosen, M.R., Miser, D.E., Starcher, M.A., Warren, J.K., 1989. Formation of dolomite in the Coorong Region, South Australia. Geochim. Cosmochim. Acta 53, 661–669.

Sánchez-Moya, Y., Sopeña, A., Ramos, A., 1996. Infill architecture of a nonmarine half-graben Triassic basin (central Spain). J. Sediment. Res. 66, 1122–1136.

Schlische, R.W., 1992. Structural and stratigraphic development of the Newark extensional basin, eastern North-America — evidence for the growth of the basin and its bounding structures. Geol. Soc. Amer. Bull. 104 (10), 1246–1263.

Schlische, R.W., 1993. Anatomy and evolution of the Triassic–Jurassic continental rift system, eastern North-America. Tectonics 12 (4), 1026–1042.

Schneider, J., Zajíc, J., 1994. Xenacanthiden (Pisces, Chondrichthyes) des mitteleuropäischen Oberkarbon und Perm- Revision der Originale zu Goldfuss 1847, Beyrich 1848, Kner 1867 und Fritsch 1879–1890. Freib. Forsch.hefte, R. C 452, 101–151.

Scholz, C.A., 1995. Deltas of the Lake Malawi Rift, East Africa: seismic expression and exploration implications. AAPG Bull. 79 (11), 1679–1697.

Scholz, C.A., Rosendahl, B.R., 1990. Coarse-clastic facies and stratigraphic sequence models from lakes Malawi and Tanganyika, East Africa. AAPG Mem. 50, 151–168.

Sclater, J.G., Christie, P.A.F., 1980. Continental stretching: an explanation of the post Mid-Cretaceous subsidence of the central North Sea Basin. J. Geophys. Res. 85, 3711–3739.

Shanley, K.W., McCabe, P.J., 1994. Perspectives on the sequence stratigraphy of the continental strata. AAPG Bull. 78, 544–568.

Šimůnek, Z., 1997. Fytopaleontologie rudnického obzoru. (in Czech). Environmental changes at the Carboniferous/Permian boundary and their impact on the floral and faunal assemblages of the fossiliferous lacustrine horizons of the Krkonoše Piedmont Basin. In: Blecha, M., Martínek, K., Drábková, J., Šimůnek, Z., Zajíc, J. (Eds.), Final report, project GAČR 205/94/0692, Czech Geological Survey, Prague, Czech Republic, pp. 79–94 (in Czech).

Slaughter, M., Hill, R.J., 1991. The influence of organic matter in organogenic dolomitization. J. Sediment. Petrol. 61, 296–303.

Sneh, A., 1979. Late Pleistocene fan-deltas along the Dead Sea rift. J. Sediment. Petrol. 49, 541–551.

Soreghan, M.J., Cohen, A.S., 1996. Textural and compositional variability across littoral segments of Lake Tanganyika: the effect of asymmetric basin structure on sedimentation in large rift lakes. AAPG Bull. 80, 382–409.

Soreghan, M.J., Scholz, C.A., Wells, J.T., 1999. Coarse-grained, deep-water sedimentation along a border fault margin of Lake Malawi, Africa: seismic stratigraphic analysis. J. Sediment. Res. 69, 832–846.

Spears, D.A., 1965. Boron in British Carboniferous sedimentary rocks. Geochim. Cosmochim. Acta 29, 315–328.

Stager, J.C., Mayewski, P.A., Meeker, L.D., 2002. Cooling cycles, Heinrich event 1, and the desiccation of Lake Victoria. Palaeogeogr. Palaeclimatol. Palaeoecol. 183, 169–178.

Stewart, A.D., Parker, A., 1979. Paleosalinity and environmental interpretation of red beds from the Late Precambrian ("Torridonian") of Scotland. Sediment. Geol. 22, 229–241.

Sweet, M.L., 1999. Interaction between aeolian, fluvial and playa environments in the Permian Upper Rotliegend Group, UK southern North Sea. Sedimentology 46, 171–187.

Talbot, M.R., 1990. A review of the paleohydrological interpretation of carbon and oxygen isotopic ratios in primary lacustrine carbonates. Chem. Geol. 80, 261–279.

Talbot, M.R., Johannessen, T., 1992. A high-resolution paleoclimatic record for the last 27,500 years in tropical west Africa from the carbon and nitrogen isotopic composition of lacustrine organic-matter. Earth Planet. Sci. Lett. 110, 23–37.

Talbot, M.R., Kelts, K., 1990. Paleolimnological signatures from carbon and oxygen isotopic ratios in carbonates from organic carbon-rich lacustrine sediments. AAPG Mem. 50, 99–112.

Talbot, M.R., Livingstone, D.A., 1989. Hydrogen index and carbon isotopes of lacustrine organic matter as lake level indicators. Palaeogeogr. Palaeoclimatol, Palaeoecol. 70, 121–138.

Talbot, M.R., Morley, C.K., Tiercelin, J.J., Le Herisse, A., Potdevin, J.L., Le Gall, B., 2004. Hydrocarbon potential of the Meso–Cenozoic Turkana Depression, northern Kenya. II. Source rocks: quality, maturation, depositional environments and structural control. Mar. Pet. Geol. 21, 63–78.

Tásler, R., Havlena, V., Prouza, V., 1981. New lithostratigraphical division of the central and western part of the Krkonoše Piedmont Basin. Věstn. Ústřed. Úst. Geol. 56, 129–143 (in Czech with English Abstr).

Taylor, G.H., Teichmuller, M., Davis, A., Diessel, C.F.K., Littke, R., Robert, P., 1998. Organic Petrology. Gebruder Borntraeger, Berlin and Stuttgart, p. 704.

Teranes, J.L., McKenzie, J.A., Lotter, A.F., Sturm, M., 1999. Stable isotope response to lake eutrophication: calibration of high-resolution lacustrine sequence from Baldeggersee, Switzerland. Limnol. Oceanogr. 44, 320–333.

Tiercelin, J.-J., Mondeguer, A., 1991. The geology of the Tanganyika Trough. In: Coulter, G.W. (Ed.), Lake Tanganyika and its Life. Oxford University Press, Oxford, pp. 7–48.

Tissot, B., Welte, D.H., 1984. Petroleum Formation and Occurrence, 2nd ed. Springer-Verlag, Berlin.

Trauth, M.H., Deino, A., Strecker, M.R., 2001. Response of the East African climate to orbital forcing during the last interglacial (130–117 ka) and the early last glacial (117–60 ka). Geology 29, 499–502.

Tucker, M.E., Wright, V.P., 1990. Carbonate Sedimentology. Blackwell, London.

Uličný, D., 1989. Boron and the organic carbon-to-reduced sulphur ratio in the Peruc–Korycany Formation (Cenomanian), Bohemia. Věstn. Ústřed. Úst. Geol. 64, 121–128.

Wells, J.T., Scholz, C.A., Soreghan, M.J., 1999. Processes of sedimentation on a lacustrine border-fault margin: interpretation of cores from Lake Malawi, East Africa. J. Sediment. Res. 69, 816–831.

Zajíc, J., 1997. Zoopaleontology of Rudník Horizon. (in Czech). In: Blecha, M., Martínek, K., Drábková, J., Šimůnek, Z., Zajíc, J. (Eds.), Environmental Changes at the Carboniferous/Permian Boundary and their Impact on the Floral and Faunal Assemblages of the Fossiliferous Lacustrine Horizons of the Krkonoše Piedmont Basin. Final report, project GAČR 205/94/0692, Czech Geological Survey, Prague, Czech Republic, pp. 94–104 (in Czech).